DOI:10.14753/SE.2024.2880

SEMMELWEIS EGYETEM

DOKTORI ISKOLA

Ph.D. értekezések

2880.

CSORBA ANITA

Szemészet
című program

Program- és témavezető: Dr. Nagy Zoltán Zsolt, egyetemi tanár

DOI:10.14753/SE.2024.2880

MICROSTRUCTURAL IMAGING EXAMINATIONS OF THE CORNEA

Ph.D. thesis

Anita Csorba

Károly Rácz Doctoral School of Clinical Medicine

Semmelweis University

Supervisor: Zoltán Zsolt Nagy, MD, D.Sc.

Official reviewers: Ágnes Kerényi, MD, Ph.D.
Szilvia Sisa-Vajda, MD, Ph.D.

Head of the Complex Examination Committee: Judit Fidy, MD, D.Sc.

Members of the Complex Examination Committee:
Miklós Dénes Resch, MD, Ph.D.
Tibor Milibák, MD, Ph.D.
András Papp, MD, Ph.D.

Budapest
2023

DOI:10.14753/SE.2024.2880

Table of Contents

DOI:10.14753/SE.2024.2880

DOI:10.14753/SE.2024.2880

List of Abbreviations

AS-OCT	anterior segment optical coherence tomography
AUC	area under the curve
BCDVA	best corrected distance visual acuity
CCT	central corneal thickness
CD	crystal density
cGSU	corrected grey scale unit
cGSU-0-2A	corrected densitometry in the anterior layer of the 0–2 mm ring
cGSU-0-2C	corrected densitometry in the center layer of the 0–2 mm ring
cGSU-0-2T	corrected densitometry in the total layer of the 0–2 mm ring
cGSU-2-6A	corrected densitometry in the anterior layer of the 2–6 mm ring
cGSU-2-6C	corrected densitometry in the center layer of the 2–6 mm ring
cGSU-2-6T	corrected densitometry in the total layer of the 2–6 mm ring
CH	cysteamine hydrochloride
CNFD	corneal nerve fiber density
CNFL	corneal nerve fiber length
CNFW	corneal nerve fiber width
CTBD	corneal nerve fiber total branch density
CTNS	Cystinosin, Lysosomal Cystine Transporter
CXL	cross-linking
D	diopter
DCD	depth of crystal deposition
GEE	generalized estimating equations
GSU	grey scale unit
IQR	interquartile range
IVCM	in vivo confocal microscopy
K_{max}	maximum keratometry
K_{mean}	mean keratometry
LCD	Langerhans cell density
LCF	Langerhans cell field
LCM	Langerhans cell morphology
LCs	Langerhans cells
ROC	receiver operating characteristic
SBNP	subbasal nerve plexus
SD	standard deviation
ThCT	thinnest corneal thickness
UCDVA	uncorrected distance visual acuity
VKC	vernal keratoconjunctivitis
ΔcGSU-0-2A	changes in corrected densitometry in the anterior layer of the 0–2 mm ring at 12 month
ΔK_{max}	changes in maximum keratometry
ΔThCT	changes in thinnest corneal thickness

DOI:10.14753/SE.2024.2880

1. Introduction

The characteristic properties of the corneal structure provide its main functions, namely precise light refraction, transmission, and biomechanical stability. The cornea consists of five main layers, the overlying epithelium, the fibrous meshwork of Bowman's layer, the stroma that composes 90% of its thickness, the Descemet's membrane, and the single layer of endothelial cells. The highly organized morphological arrangement of the cellular and extracellular constituents of these layers, the avascular nature, and the strictly governed physiological hydration are all essential for maintaining optical clarity. The transparent architecture not only ensures adequate light transmittance but also makes the cornea excellently suitable for examination of its morphology with various optical devices. In the last decades, clinical imaging modalities for examining the living human cornea underwent significant development. With contemporary imaging techniques, the in vivo visualization of the delicate structural appearance became possible, even at the cellular level. Since corneal diseases are usually associated with morphological abnormalities, modern imaging techniques that are capable of imaging structural changes can contribute to a more accurate understanding of various disease processes. Scheimpflug imaging, in vivo confocal microscopy (IVCM), and anterior segment optical coherence tomography (AS-OCT) are among the current main tools for examining corneal microstructures and are increasingly a key part of the clinical assessment of corneal diseases.

The Scheimpflug technique is a commonly used modality in corneal imaging. The Scheimpflug principle states that the subject plane, the lens plane, and the film planes are not parallel to one another, thus they intersect in a common straight line. Therefore, this method extends the depth of focus and enhances the sharpness of points in the image that are situated in different planes, while minimizing distortion across the image, which results in a tomogram with excellent sharpness (1). The most common Scheimpflug devices include Pentacam HR, which ensures noncontact imaging of the anterior segment from the anterior surface of the cornea to the posterior surface of the lens and provides cross-sectional scans. The scans are produced by a 360° rotating camera, which uses monochromatic blue light with 475 nm wavelength. With Pentacam HR, optical densitometry measurement can be performed, which means that the device can measure the backward corneal light scattering (2). Using the 'Cornea Densito' software, the degree

and location of corneal opacities, such as corneal haze, can be quantified objectively in concentric rings and in different depth layers of the cornea.

IVCM provides real-time, noninvasive visualization of living human tissues at the cellular level and morphological assessment of the represented structures. This device uses a laser light source and is based on the principle of the confocality of the object with the light source and the detector plane. Specifically, the illumination and the detection optics are focused on the same diffraction-limited spot, while the out-of-plane backscattered light signals are suppressed, thus, the image is contributed solely by the object layer present at the focal plane (3). As a consequence, the confocal technique provides imaging with high magnification, a lateral resolution of 1−2 μm/pixel and an axial resolution of 4–10 μm/pixel (3, 4). This modality allows the subsurface imaging of examined tissues in their native state, thus, it provides an 'optical biopsy'. Confocal images present the morphological architecture in an *en face* plane since the plane of the image is parallel to the surface of the examined structure (3). IVCM is mainly used in the field of research on corneal pathology since it is excellent for the in vivo morphological visualization of all layers of the cornea in full thickness (5).

AS-OCT is a relatively novel imaging technique for detailed analysis of the anterior structures of the eye including the cornea. It uses low-coherence interferometry, while the light reflected from the examined tissue interferes with a reference light beam, and the interference pattern can be measured. This results in cross-sectional images of the examined tissue with high resolution, which allows us to image corneal layers and structures in great detail. AS-OCT provides rapid acquisition speed and contactless imaging. Therefore, it is preferable for patients with low compliance regarding contact corneal examinations, such as IVCM (6).

Accordingly, the above-mentioned contemporary imaging tools have a prominent role in many aspects of corneal structural examinations. These devices are beneficial in the investigation of the pathophysiology and course of various inflammatory or degenerative corneal disorders or even the impacts of surgeries. In the present thesis, the objective was to present innovative data obtained through the investigation of three distinct corneal pathologies. The common features of these diverse pathologies is that they are all accompanied by characteristic microstructural changes in the cornea.

1.1. Cross-linking therapy

Keratoconus is a bilateral ectatic corneal disorder with progressive protrusion and thinning. As a consequence, irregular astigmatism and deterioration of visual acuity may develop (7). The most effective method to prevent ectatic progression is the application of minimal-invasive corneal collagen cross-linking (CXL) therapy (8). CXL utilizes the combination of photosensitizing riboflavin and ultraviolet-A light to form crosslinks between collagen fibrils, inducing increased corneal rigidity after treatment (9). Although, CXL is a safe and effective technique to increase the stability of the cornea in progressive keratoconus, it may induce stromal haze formation (8). Previous studies demonstrated that CXL can produce various cellular changes that might impair corneal transparency (10, 11). In the initial postoperative period, keratocyte apoptosis and edematous, hyperreflective extracellular stroma can be observed. These changes may persist for up to 6 months but generally resolve by 12 months after the procedure, followed by the disappearance of haze (11). Corneal haze can be quantified with the above-mentioned optical densitometry measurement. Previous studies have already evaluated correlations between densitometry values and postoperative outcomes, however, the relationship between the predictive factors of postoperative corneal haze formation has not been elucidated yet. Furthermore, the impact of stromal haze on the postoperative results is also controversial (12-14).

1.2. Vernal keratoconjunctivitis

Vernal keratoconjunctivitis (VKC) is a severe type of allergic inflammation of the cornea and conjunctiva that mainly affects young boys during childhood and usually resolves after puberty (15, 16). In general, the symptoms may persist for 4 to 8 years and present with seasonal exacerbations, although the perennial form is not uncommon, particularly in subtropical climates (15, 17-19). VKC may occur in either an active or quiescent form, with varying symptom severity and diversity. During the active phase, the disease is characterized by intense and persistent itching, tearing, photophobia, conjunctival redness, chemosis, and fibrinous discharge (18). Severe cases may also cause superficial punctate keratopathy, macro-erosions, shield ulcers, plaque formation, corneal scarring, and neovascularization (15, 17, 18, 20). The giant papillae in the upper tarsal conjunctiva and limbal gelatinous opacifications (Trantas' dots) are characteristic

symptoms (18, 21). Although the giant papillae become severely swollen during exacerbations, they may also persist in-long term during the quiescent phase of the disease without signs of any inflammation (16, 18). According to recent studies, even in patients with quiescent VKC without any inflammatory signs, some alterations can still be detected. These changes include overexpression of proinflammatory proteins in tear samples and subclinical tear film dysfunction, which may suggest a sustained inflammatory shift in the ocular surface milieu (22-25). To date, there are only a limited number of studies that have investigated corneal morphology using IVCM in VKC patients, and these reports have focused on morphological changes during active inflammation or after local therapy (26-29). Our research was the first to report data on the microstructural alterations that may occur during the quiescent phase of the disease (30).

1.3. Ophthalmological aspects of nephropathic cystinosis

Cystinosis is an autosomal recessively inherited rare lysosomal storage disease. The disease is caused by a mutation in the CTNS (Cystinosin, Lysosomal Cystine Transporter) gene, which is located at the 17p13.2 chromosome (31). The CTNS gene encodes for cystinosin, a transmembrane protein transporter that transports cystine amino acids out of the lysosome. Due to the mutation, the level of intralysosomal cystine progressively increases, and it forms insoluble crystals (32). These crystal deposits appear in different tissues and cause functional impairment of organs, particularly the kidneys and eyes (33, 34). Nephropathic or infantile cystinosis is the most common (accounting for 95% of cases) and severe phenotype (35). Children with nephropathic cystinosis usually require renal transplantation already in the first decade of their life (33). In this phenotype, the eyes are severely affected by crystal deposition (31). Although the deposition occurs in all ocular structures, the most notable manifestation is the accumulation of cystine crystals in the cornea (6). Corneal crystal deposition results in marked photosensitivity, blepharospasm, and dry eye, although the visual acuity usually remains preserved (36). IVCM is the gold standard imaging method for the quantification and identification of crystal deposits at the cellular level (31). Despite AS-OCT being faster and less inconvenient for patients, very few studies have utilized AS-OCT for the analysis of corneal morphology in patients with cystinosis (6, 36). In the nephropathic

form, by slit-lamp biomicroscopy, the crystal deposits can be detected from the age of 16 months, and a continuous increase of the amount of deposits can be observed with age (36, 37). Previous studies have shown contradictory results regarding the most affected corneal layer by crystal deposition, however, the reason for this discrepancy has not been clarified yet (35, 38-40). Additionally, no prior research has investigated whether the age of patients has any relationship with corneal crystal morphology and arrangement.

DOI:10.14753/SE.2024.2880

2. Objectives

The objective of my research was to investigate the corneal microstructure in different corneal disorders, i.e., in patients with CXL-treated keratoconus, in patients with quiescent vernal keratoconjunctivitis, and in patients with nephropathic cystinosis. In order to accomplish these objectives, the aims of the presented studies were the followings:

1. **Effects of conventional CXL therapy in progressive keratoconus**
   (i). To characterize the main postoperative outcomes including corneal haze, curvature, and thickness during a one-year follow-up period after CXL treatment in patients with progressive keratoconus using a Scheimpflug-camera.
   (ii). To analyse the relationship between preoperative parameters (e.g., age, pachymetry, and keratometry), and their postoperative changes with corneal flattening and haze formation, and analyse the associations between postoperative haze and visual outcome.
2. **Corneal microstructural alterations of patients with quiescent vernal keratoconjunctivitis**
   (i). To analyse whether some corneal changes may be observed during the quiescent phase of VKC compared to normal eyes using IVCM.
   (ii). To determine the influencing factors of the morphology and density of corneal Langerhans cells.
3. **Corneal alterations in nephropathic cystinosis**
   (i). To analyse the corneal architecture and the characteristics of crystal arrangement in different corneal layers in nephropathic cystinosis using IVCM and AS-OCT.
   (ii). To assess the crystal arrangement in terms of patients' age.

3. Methods

3.1. Analysis of the effects of conventional cross-linking in progressive keratoconus

3.1.1. Study design and subjects

The study was performed at the Department of Ophthalmology, Semmelweis University, with approval from the Semmelweis University Regional and Institutional Committee of Sciences and Research Ethics (SE-RKEB-104/2020). All involved participants were informed about the treatments and written consent was obtained. All examinations were carried out in accordance with the tenets of the Declaration of Helsinki. Our study included 47 patients with progressive keratoconus who underwent conventional CXL between 2017 and 2018. Surgical intervention was indicated when ectatic progression (i.e., an increase of ≥ 1.0 diopter in maximum keratometry values (K_{max}) or a loss of ≥ two lines of best corrected distance visual acuity (BCDVA) in 1 year) was observed (41). The distribution of the cohort according to the severity of the keratoconus was demonstrated based on the Amsler-Krumeich classification (42). Patients under 18 years of age, those with preoperative corneal scarring, previous corneal hydrops or keratitis, history of any eye injury, or corneal thickness below 400 μm were excluded. All pre- and postoperative data were collected and analysed in a retrospective manner.

3.1.2. Surgical procedure

Conventional epithelium-off corneal CXL was performed by the same surgeon (Z.Zs.N.) according to Dresden protocol (43). Prior to surgery, 0.4% oxybuprocaine eye drops (Benoxi®, Unimed Pharma, Bratislava, Slovakia) were administered topically into the inferior conjunctival cul-de-sac. The central 8 mm diameter of the corneal epithelial layer was mechanically removed with a blunt spatula, and 0.1% riboflavin droplets (Medio-Haus Medizinprodukte GmbH, Rostock, Germany) were topically applied every 2 minutes for the next 30 minutes. Afterward, ultraviolet-A light with a wavelength of 370 ± 5 nm (CSO Vega CMB X Linker, CSO Scandicci, Firenze, Italy) was then directed onto the corneal surface from a distance of 1 cm for 30 minutes with continued administration of riboflavin droplets in every 2 minutes, at an irradiance of 3 mW/cm^2 intensity. Finally, topical antibiotic drops (5 mg/ml levofloxacin) were administered, and

a bandage was applied. In the early postoperative period, all patients were examined on the first day after the surgery, when the bandage was removed, and 1 week later. Antibiotic drops (5 mg/ml levofloxacin) were instilled five times daily during the first postoperative week. Following the complete re-epithelialization of the cornea, topical corticosteroid eye drops (1 mg/ml fluorometholone) was administered four times per day for one month.

3.1.3. Ophthalmological examinations

Ophthalmological examinations included uncorrected distance visual acuity (UCDVA) and BCDVA assessment (measured with Snellen chart and converted to logMAR values). Slit-lamp biomicroscopy and Scheimpflug imaging (Pentacam HR, Oculus Optikgeräte GmbH, Wetzlar, Germany) were performed in each case before the surgery and at 1, 3, 6, and 12 months after the CXL procedure. The thinnest corneal thickness (ThCT), the K_{max}, the mean keratometry values (K_{mean}), and the corneal densitometry values in different rings and depth layers were recorded. Regarding the Scheimpflug images, only measurements with good image quality were considered acceptable, as indicated by the "OK" note in the quality specification window.

The ’Cornea Densito’ module displays a chart including the average corneal densitometry values given in grey scale units (GSU; 0–100 light scattering; 0: maximal transparency/optically clear cornea; 100: minimal transparency/total corneal opacification) in four concentric rings (0–2 mm; 2–6 mm; 6–10 mm; 10–12 mm) and in three layers in different depths. The „Anterior” layer represents the front 120 μm, while the „Posterior” refers to the hind 60 μm of the full corneal thickness. The „Center” layer provides the values between the aforementioned two layers, hence, the thickness of this layer varies for each patient. The "Total" layer displays the average optical density of the entire corneal thickness. Since different rings have different surface areas and thicknesses, an additional calculation was performed as follows: raw densitometry data in GSU were converted to GSU/cubic millimeter (GSU/mm^3), as previously published by Nemeth *et al.* (44). Initially, we calculated values in GSU/mm^2 with dividing raw GSU data of each concentric ring by its area (3.141 mm^2 for ring 0–2 mm; 25.132 mm^2 for ring 2–6 mm; 50.265 mm^2 for ring 6–10 mm; 34.557 mm^2 for ring 10–12 mm and 78.539 mm^2 for total diameter). The values of different rings in GSU/mm^2 were then divided by the

thickness of the appropriate layer in mm (0.12 mm for the anterior layer and 0.06 for the posterior layer). The thickness of the center layer was calculated by subtracting 120 μm and 60 μm from the total thickness which was recorded from the „Pachy apex" window (the *X* and *Y* coordinates of this point are 0.00) and then it was converted to mm. With this additional calculation, we got surface area- and thickness-corrected densitometry values in GSU/mm^3 (cGSU).

3.1.4. Statistical analysis

The statistical analysis was carried out utilizing IBM® SPSS® Statistics 25.0 software (IBM Corp. ©Copyright IBM Corporation). The Kolmogorov-Smirnov test was employed to test the normality of the variables. Based on its results, changes in UCDVA, BCDVA, keratometry, pachymetry, and densitometry were assessed using the nonparametric Friedman test. When the Friedman test yielded statistical significance, post hoc pairwise comparison was conducted using the Wilcoxon signed-rank test to compare each time point to the baseline (i.e., baseline vs. 1 month, baseline vs. 3 months, baseline vs. 6 months, and baseline vs. 12 months). As these four analyses were conducted for each repeated testing procedure, a Bonferroni-adjusted significance level was applied for each comparison resulting in a significance level at p <0.0125. Additionally, a receiver operating characteristic (ROC) curve was plotted to identify the most characteristic densitometry data for corneal haze formation at the 12-month follow-up visit. A comparison of ROC curves was performed to test the statistical significance of the difference between the areas under the curves (AUC) with the method of DeLong *et al*. using MedCalc®, version 19.4.1. (MedCalc Software Ltd., Ostend, Belgium) (45). The Spearman's rank correlation test was utilized to identify the associations between preoperative parameters (age, pachymetry, and keratometry) and their postoperative changes, and in haze formation and corneal flattening (difference between the postoperative 12-month value and the preoperative value). The associations of postoperative visual acuity (dependent variable of interest) with the densitometry values (independent variable) 1 year after surgery were assessed with generalized estimating equations (GEE). Preoperative maximum keratometry was incorporated as a covariate in the regression model to adjust for potential confounding. The level of significance was considered at p <0.05 in all analysis, except the post hoc Wilcoxon test.

3.2. Examination of corneal microstructural alterations of patients with quiescent vernal keratoconjunctivitis

3.2.1. Study design and subjects

This study was conducted at the Department of Ophthalmology, Semmelweis University. The study protocol was approved by the Semmelweis University Regional and Institutional Committee of Sciences and Research Ethics (SE-RKEB-4/2019). All examinations were conducted in accordance with the Declaration of Helsinki, and all participants were treated in an ethical, responsible, and safe manner. Informed consent was obtained from the parents or legal guardians of participants under the age of 18.

A total of 20 subjects with a history of VKC were involved in this study. The severity of the symptoms was graded, and only patients with grade 0 (quiescent phase, no symptoms) were included in the study (15, 18). Patients were included if they had an active phase of VKC for at least two seasons in their medical history, and their last active phase occurred in the spring or summer season before participating in the study. Patients with systemic diseases, active VKC, significant dry eye requiring continuous tear supplementation, or any history of abnormal corneal disorders (such as keratoconus, scarring, neovascularization, or parakeratosis), or those who wore contact lenses were excluded. In the VKC group, previously prescribed local therapies included the combination of preservative-free artificial tear drops, topical dual-acting agents (olopadatine), antibiotics (tobramycin) in the case of corneal involvement, and potent corticosteroids (dexamethasone) as a short, pulse therapy during the severe acute inflammation. During the active phase, as a maintenance treatment for the prevention of severe recurrence, all patients used preservative-free artificial tear drops; and among them, 7 combined it with dual-acting agents (olopatadine), 2 with dual-acting agents and low potent corticosteroid (fluorometholone) and 11 with calcineurin-inhibitor (cyclosporine-A). At the time of the examinations, all involved patients had abstained from medication for at least two months. A control group of 25 healthy volunteers, matched by age and gender, was also enrolled. The control subjects had no history of systemic or ocular disease. Demographic and clinical parameters, including age, gender, duration of the disease, length of the quiescent phase, and personal and family history of atopy, were recorded for all participants.

3.2.2. Ophthalmological examinations

Initially, a conventional slit-lamp biomicroscopy examination was performed to assess the severity of upper tarsal papillary hypertrophy using the Bonini scale (ranges from 0 to 3: 0, no papillary reaction; 1, mild-; 2, moderate-; 3, severe papillary reaction) as previously published (18). Subsequently, the IVCM imaging of the cornea was performed using the Rostock Cornea Module of Heidelberg Retina Tomograph-III (Heidelberg Engineering GmbH, Heidelberg, Germany) with a 400 µm field of view lens. Prior to the examination, 0.4% oxybuprocaine (Benoxi®, Unimed Pharma, Bratislava, Slovakia) was instilled locally in the lower cul-de-sac. A sterile polymethyl methacrylate cap (TomoCap®, Heidelberg Engineering GmbH) was placed over the microscope lens and one drop of artificial tear gel (0.2% carbomer, Vidisic®, Chem.-pharm.Fabrik GmbH, Brunsbütteler, Berlin, Germany, Bausch&Lomb) was applied on the top to ensure airless contact. The instrument's section mode was utilized to record images of each layer in the full thickness of the central cornea, from the epithelium to the endothelium. Each IVCM image represented an *en face* section of the cornea with a resolution of 384 × 384 pixels covering a 0.4 × 0.4 mm^2 area.

3.2.3. Image analysis

In order to eliminate inter-observer variability, IVCM images were analysed by the same examiner (A.Cs.) in a masked manner. The in-built Cell Count function was used to assess the cell density (number of cells/mm^2) of the epithelial wing and basal cells, Langerhans cells (LCs), keratocytes in the anterior, middle, and posterior stromal layer, and endothelium, after manually marking the cells. Three high-contrast, nonoverlapping images representing a single corneal layer were selected and analysed from the different layers. Then, the cell density values of the three records were averaged. ACCMetrics software (version 2.0; University of Manchester, Manchester, UK) was used to analyse the morphology of the subbasal nerve plexus (SBNP). This software automatically quantifies the following nerve fiber parameters: corneal nerve fiber density (CNFD, the number of fibers/mm^2); corneal nerve fiber length (CNFL, the total length of nerves mm/mm^2); corneal nerve fiber total branch density (CTBD, the total number of branch points/mm^2) and corneal nerve fiber width (CNFW, the average nerve fiber width mm/mm^2). A set of nonoverlapping images with good quality (between 3–13) including

the SBNP was selected per eye and was analysed by using multiple image analysis mode. For each eye, the data from the image with the highest CNFL value was selected (46). Using that certain image, the tortuosity of SBNP was evaluated according to the previously published Oliveira-Soto and Efron score on a scale from 0 to 4 (47).

The presence of microscopic signs of ocular inflammation was also in the focus of our investigation. LCs were identified as hyperreflective corpuscular structures with or without dendritic processes located at the level of basal epithelium and at the SBNP. Three nonoverlapping images representing LCs were selected for evaluation. The morphology of LCs (LCM) was assessed according to a 0–3 scale as previously published as follows: score 0, no LCs are represented; score 1, LCs without processes; score 2, LCs with small processes and score 3, LCs with long processes (48-51). The same three images were employed for the analysis of LCs density (LCD), and an average value was calculated for each participant. Quantification of certain parameters of LC morphology was also performed using the Image J software (version 1.53c, National Institutes of Health, USA). To determine the size of the LCs, the Langerhans cell field (LCF) area (μm^2) was calculated. This measurement is indicative of the size of the cell body and the dendrite length and was obtained by measuring the polygon area formed by connecting the outermost endpoints of the dendrites of each LC (52, 53). For this measurement, a systematic approach was used to prevent any potential bias in the selection of LCs. LCs were scored and quantified in a consecutive manner, beginning from the top left-hand corner of the IVCM image, until a maximum of 20 unique corneal LCs per participant were identified, as previously described (52). Leukocyte occurrence was assessed in both the epithelium and anterior stroma (3, 54). Additionally, signs of keratocyte activation (larger size, round shape, higher reflectivity of cell nucleus, and inhomogeneous background reflectivity) in the anterior stroma were evaluated.

3.2.4. Statistical analysis

The statistical analysis was performed using IBM® SPSS® Statistics 27.0 software (IBM Corp. ©Copyright IBM Corporation). A Chi-square test was utilized to evaluate the gender ratio between VKC patients and the control group. The normality of the variables was tested using the Shapiro-Wilk test. Differences in variables between the VKC and control group were analysed using the independent t-test for normally

distributed data and the Mann-Whitney U test for nonnormally distributed data. In the VKC group, a regression analysis was conducted to determine the associations between the density and morphology of LCs (dependent parameters) and associated factors via GEE. Age, gender, personal or family history of atopy, length of the quiescent phase, disease duration, and the severity of papillary hypertrophy were supposed to be the potential associated factors. Initially, univariable modeling was conducted to identify variables that displayed a significant association with the dependent parameter. Subsequently, all variables that were found to be significantly associated were incorporated as covariates in the regression model. Variables were retained in the model if they were associated with a *p*-value less than 0.05. For all statistical analyses, the statistical significance level was defined as $p < 0.05$.

3.3. Examination of the corneal alterations in nephropathic cystinosis

3.3.1. Study design and subjects

A cross-sectional study was carried out at the Department of Ophthalmology, Semmelweis University with the approval of the Semmelweis University Regional and Institutional Committee of Sciences and Research Ethics (SE-RKEB-224/2018). Prior to participation, all individuals were informed about the details of the study and written consent was obtained from either the patients or the parents or legal guardians of participants under 18 years of age. The study adhered to the principles of the Declaration of Helsinki.

In our study, six patients diagnosed with nephropathic cystinosis, consisting of 4 males and 2 females ranging in age from 8 to 36 years were included. All enrolled patients had been diagnosed with nephropathic cystinosis previously and had corneal crystals observed during a slit-lamp examination. All subjects were receiving oral cysteamine bitartrate (Cystagon®, Orphan Europe S.A.R.L., Puteaux, France) as a systemic treatment and were also regularly applied topical 0.1% cysteamine hydrochloride (CH) eye drops (obtained from the University Pharmacy Department of Pharmacy Administration, Budapest, Hungary) once to four times daily.

3.3.2. Ophthalmological examinations

Initially, all patients underwent a comprehensive ophthalmological examination, which included an assessment of BCDVA (measured with a Snellen chart and converted to logMAR values) followed by slit-lamp biomicroscopy. Subsequently, patients underwent AS-OCT examinations using AngioVue OCT (RTVue-XR, Avanti, Optovue, Fremont, CA, USA), which provided 12 × 9 mm scans with an axial resolution of 5 μm and a transversal resolution of 15 μm. Finally, IVCM analysis of the central cornea was performed with the Rostock Cornea Module of Heidelberg Retina Tomograph-III (Heidelberg Engineering GmbH, Heidelberg, Germany), with the same method as previously described in section *3.2.2.*

3.3.3. Image and data analysis

On the AS-OCT images, the depth of crystal deposition (DCD) was measured with the caliper function. This means that the distance from the anterior corneal surface to the deepest point of crystal deposition at the center of the cornea was determined. The software automatically measured central corneal thickness (CCT) values, which were derived from the pachymetry map. On the IVCM images, the crystal density (CD) was quantified using a CD scoring system according to Labbé *et al*. as previously published (36). The CD was evaluated based on standard images in the following four different corneal layers: epithelium, anterior stroma, posterior stroma, and endothelium. Each image was graded from 0 to 4 (graded from 0 to 4: 0, no crystal; 1, <25%; 2, 25% to 50%; 3, 50% to 75%; 4, >75%; the percentage was determined based on the quotient of the area affected by crystal deposition and the whole field of each image). The CD for one corneal layer represented the mean of five separate, nonoverlapping images. The values of DCD and CD were evaluated for patients of different ages. Due to the low number of patients, no statistical analysis was performed.

4. Results

4.1. Effects of conventional cross-linking therapy in progressive keratoconus

4.1.1. Patients' characteristics

This study involved 47 eyes of 47 patients with keratoconus who underwent conventional CXL therapy, including 35 male and 12 female subjects with a mean age of 26.72 ± 6.03 (range, 18–38) years before CXL. All involved patients were Caucasian. Regarding the distribution of keratoconus severity, the cohort was comprised of 21 eyes (44.7%) in stage I, 19 eyes (40.4%) in stage II, and 7 eyes (14.9%) in stage III (42). During the follow-up period, no ophthalmological complications were observed as a result of the CXL surgery.

4.1.2. Postoperative outcomes

The Friedman test showed statistically significant changes in both UCDVA and BCDVA after CXL (all p <0.001). In terms of UCDVA, a significant difference was observed at 1 month compared to baseline (post hoc p = 0.005). At 1-, 3-, and 6-month, BCDVA was lower compared to the preoperative values (post hoc p >0.0125), but the difference was statistically significant only also at the first postoperative month (post hoc p = 0.005). At 12 months, there was no significant difference compared to the baseline value neither in UCDVA nor in BCDVA (post hoc p = 0.041 and p = 0.438) (Table 1).

The Friedman test demonstrated significant changes in K_{max}, K_{mean}, and ThCT values postoperatively (all p-values <0.001). Post hoc analysis revealed a significant increase in the K_{max} value 1 month after surgery, with a peak value of 57.15 ± 5.74 diopters (D), compared to the preoperative value of 56.41 ± 5.41 D (post hoc p <0.001). Thereafter, keratometry readings began to decrease. At the 1-year follow-up, K_{max} values decreased significantly to 55.35 ± 5.18 D compared to baseline (post hoc p <0.001). Change in K_{mean} showed a similar trend with significant changes at 3, 6, and 12 months (post hoc p <0.001). The average decrease in K_{max} value (ΔK_{max}) was -1.05 ± 1.13 D, and it was -0.71 ± 0.78 D in K_{mean} during the follow-up period. A significant decrease in ThCT was observed in all postoperative months examined compared to the preoperative value (all post hoc p-values <0.001), with an average decrease of -15.5 ± 15.19 μm observed one year after treatment (Table 1).

Table 1. Uncorrected- and best corrected distance visual acuity (UCDVA and BCDVA, logMAR), thinnest corneal pachymetry (ThCT, μm), maximum and mean keratometry (K_{max} and K_{mean}, diopters) at certain follow-up visits. *Statistically significant difference compared to baseline (Bonferroni-adjusted post hoc *p*-value <0.0125). Data are shown as mean ± standard deviation.

Variables	Preoperative	Postoperative			
		1 months	3 months	6 months	12 months
BCDVA (logMAR)	0.16 ± 0.2	0.23 ± 0.21*	0.18 ± 0.19	0.18 ± 0.18	0.13 ± 0.2
UCDVA (logMAR)	0.56 ± 0.38	0.64 ± 0.35*	0.56 ± 0.35	0.55 ± 0.34	0.51 ± 0.32
ThCT (μm)	476.49 ± 34.57	444.3 ± 38.88*	451.39 ± 37.75*	455.11 ± 36.52*	460.94 ± 35.74*
K_{max} (D)	56.41 ± 5.41	57.15 ± 5.74*	56.01 ± 6.03	55.75 ± 5.67	55.35 ± 5.18*
K_{mean} (D)	47.47 ± 3.49	47.54 ±3.87	46.93 ± 3.64*	46.81 ± 3.61*	46.76 ±3.31*

Table 2 summarizes the mean cGSU values at different follow-up visits. The Friedman test revealed statistically significant changes in densitometry values of the anterior, center, and total layers of the 0–2 mm, 2–6 mm, and 6–10 mm rings after CXL (all *p*-values <0.001). Further analysis with the Wilcoxon test showed that cGSU values in the anterior, center, and total layers of the 0–2 mm and 2–6 mm rings were significantly increased at all postoperative visits (all post hoc *p*-values <0.0125). In the 6–10 mm ring, a significant increase in cGSU was found in the anterior layer at 1-, and 3-month-visit (all post hoc p <0.001) and in the center and total layers at all follow-up visits (post hoc p <0.0125). A peak in densitometry values was revealed 3 months after CXL in the most central zone and after 1 month in the 2–6 mm and 6–10 mm rings. Subsequently, the densitometry values began to decrease. Regarding the different corneal layers, the Friedman test showed significant changes in total densitometry of the anterior, center, and total layers (all p <0.001). Post hoc analysis revealed that densitometry values of these layers were significantly increased at all postoperative visits (all post hoc p <0.001) with an exception of the total densitometry of the center layer at 12 months (post hoc $p = 0.079$). Densitometry values in the remaining zones did not change significantly after CXL (all post hoc p >0.0125).

DOI:10.14753/SE.2024.2880

Table 2. Corrected densitometry values in grey scale unit per cubic millimeter (GSU/mm^3) at all postoperative months. *Statistically significant difference compared to baseline (Bonferroni-adjusted *p*-value <0.0125). †*p*-values of Friedman tests. ††Post hoc *p*-value of 12-month data compared to baseline. Data are shown as mean ± standard deviation.

Variables		Preoperative	Postoperative				$p^{\dagger}$	$p^{\dagger\dagger}$
			1 months	3 months	6 months	12 months		
Anterior	0–2 mm	79.29 ± 6.75	107.45 ± 17.86*	113.55 ± 21.8*	104.27 ± 16.86*	100.64 ± 14.06*	< 0.001	< 0.001
	2–6 mm	8.45 ± 0.66	11.07 ± 1.35*	10.71 ± 1.12*	9.76 ± 1.13*	9.4 ± 0.84*	< 0.001	< 0.001
	6–10 mm	3.39 ± 0.37	3.83 ± 0.63*	3.56 ± 0.41*	3.42 ± 0.37	3.42 ± 0.36	< 0.001	= 0.17
	10–12 mm	6.54 ± 1.87	6.23 ± 2.05	6.27 ± 2.09	6.27 ± 1.74	6.45 ± 2.23	= 0.895	
	Total	2.63 ± 0.24	3.17 ± 0.37*	3.13 ± 0.36*	2.93 ± 0.33*	2.87 ± 0.31*	< 0.001	< 0.001
Center	0–2 mm	18.74 ± 2.41	25.49 ± 5.93*	26.17 ± 8.23*	22.98 ± 5.23*	22.26 ± 9.68*	< 0.001	< 0.001
	2–6 mm	1.98 ± 0.27	2.63 ± 0.53*	2.49 ± 0.58*	2.24 ± 0.36*	2.12 ± 0.33*	< 0.001	< 0.001
	6–10 mm	0.89 ± 0.13	1.07 ± 0.27*	1.0 ± 0.18*	0.96 ± 1.16*	0.93 ± 0.15*	< 0.001	= 0.003
	10–12 mm	1.83 ± 0.53	1.86 ± 0.46	1.92 ± 0.64	1.94 ± 0.56	1.85 ± 0.5	= 0.119	
	Total	0.66 ± 0.08	0.82 ± 0.18*	0.79 ± 0.17*	0.74 ± 0.13*	0.66 ± 0.08	< 0.001	= 0.079
Posterior	0–2 mm	67.88 ± 9.33	68.98 ± 9.39	71.65 ± 13.7	66.73 ± 9.49	67.68 ± 9.03	= 0.418	
	2–6 mm	8.50 ± 0.78	10.09 ± 9.82	8.61 ± 0.74	8.24 ± 0.82	8.27 ± 0.64	= 0.032	= 0.039
	6–10 mm	4.24 ± 0.63	4.32 ± 0.78	4.23 ± 0.59	4.12 ± 0.51	4.16 ± 0.49	= 0.439	
	10–12 mm	8.43 ± 0.94	8.37 ± 1.99	8.2 ± 1.89	8.43 ± 1.83	8.61 ± 1.96	= 0.451	
	Total	2.86 ± 0.33	2.89 ± 0.38	92.87 ± 0.32	2.8 ± 0.29	2.83 ± 0.26	= 0.659	
Total	0–2 mm	13.25 ± 1.34	17.34 ± 3.92*	18.3 ± 3.92*	16.54 ± 2.81*	15.94 ± 3.02*	< 0.001	< 0.001
	2–6 mm	1.46 ± 0.14	1.89 ± 0.28*	1.88 ± 0.28*	1.65 ± 0.21*	1.58 ± 0.16*	< 0.001	< 0.001
	6–10 mm	0.64 ± 0.07	0.74 ± 0.15*	0.69 ± 0.08*	0.67 ± 0.08*	0.66 ± 0.07*	< 0.001	= 0.007
	10–12 mm	1.27 ± 0.33	1.33 ± 0.42	1.29 ± 0.38	1.29 ± 0.33	1.32 ± 0.38	= 0.473	
	Total	0.47 ± 0.05	0.57 ± 0.1*	0.56 ± 0.08*	0.52 ± 0.07*	0.51 ± 0.06*	< 0.001	< 0.001

4.1.3. Postoperative outcomes and associated parameters

For ROC analysis, significantly increased corrected densitometry data at 12 months were used from the central rings mostly affected by CXL (anterior, center, and total layer of 0–2 mm and of 2–6 mm rings). The ROC curve analysis revealed that the corrected densitometry in the anterior layer of the 0–2 mm ring (cGSU-0-2A) was the most characteristic parameter of corneal densitometry changes one year after CXL with an AUC of 0.936. AUC of cGSU-0-2A was statistically significant compared to other AUCs (cGSU-0-2C, p <0.001; cGSU-0-2T, p <0.001; cGSU-2-6A, p <0.001; cGSU-2-6C, p <0.001 and cGSU-2-6T, p <0.001, respectively) (Figure 1). Thus, the data of the cGSU-0-2A region were hereinafter used to examine the relationship between preoperative data and densitometry values. The average increase in densitometry of this region was 21.35 ± 14.69 cGSU/mm^3 as compared to the baseline.

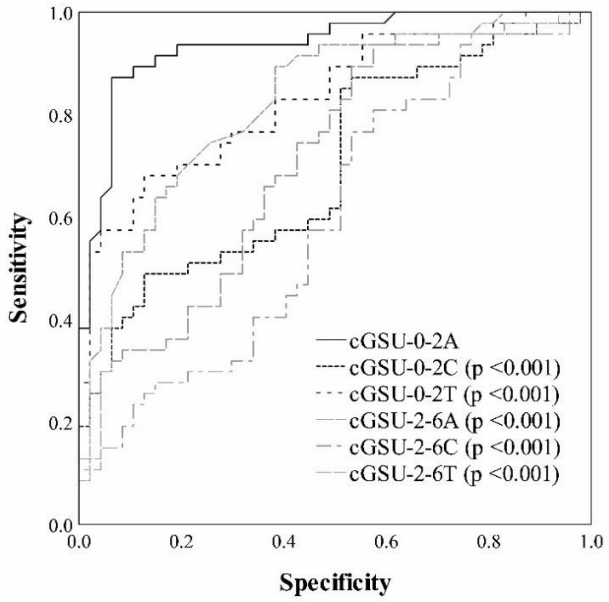

Figure 1. Receiver operator characteristic (ROC) curve analysis of densitometry data in different regions. ROC analysis determined corrected densitometry data in anterior layer of 0–2 mm ring (cGSU-0-2A) as the most sensitive parameter of corneal densitometry changes after cross-linking (CXL). All significantly increased corrected densitometry data at 12 months from the central rings mostly affected by CXL were plotted, i.e., anterior, center and total layers of 0–2 mm and of 2–6 mm rings (cGSU-0-2A, cGSU-0-2C, cGSU-0-2T and cGSU-2-6A, cGSU-2-6C, cGSU-2-6T). Comparison of AUCs showed AUC of cGSU-0-2A was statistically significant compared to other AUCs (*p*-values are shown for corresponding parameters). Own representation, published in (55).

DOI:10.14753/SE.2024.2880

After analysing the relationship between the changes in densitometry (ΔcGSU-0-2A) and the preoperative parameters, a moderate but statistically significant correlation between the changes in haze in this region and preoperative K_{max} has been found one year after CXL (R = 0.303, p = 0.038) as shown in Figure 2.

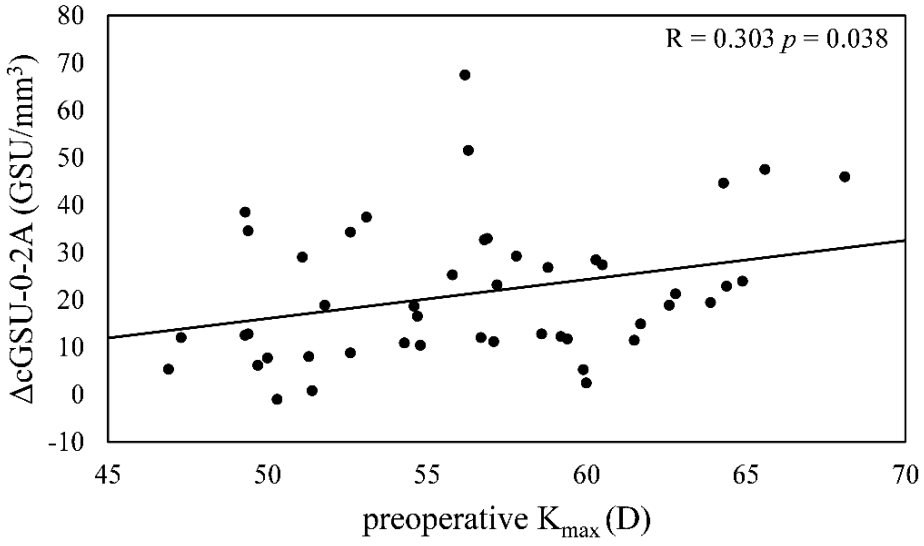

Figure 2. Relationship between the changes in haze 12 months after treatment (ΔcGSU-0-2A, GSU/mm^3) and preoperative maximum keratometry (K_{max}, diopters). Statistically significant correlation was found between ΔcGSU-0-2A and preoperative K_{max}. Own representation, published in (55).

DOI:10.14753/SE.2024.2880

At postoperative 12 months, there was a moderate significant negative correlation between ΔcGSU-0-2A and ΔK_{max} (R = -0.412, p = 0.004) as shown in Figure 3.

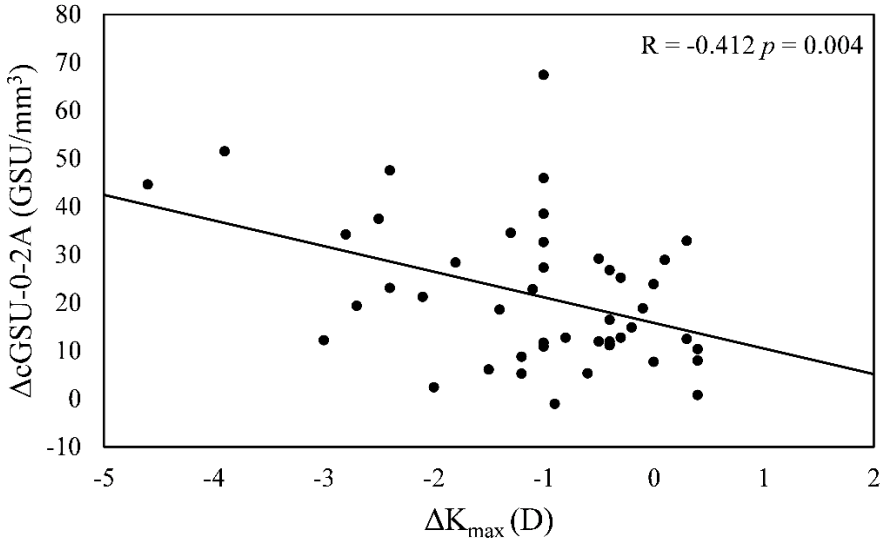

Figure 3. Relationship between changes in densitometry at 12 months (ΔcGSU-0-2A, GSU/mm^3) and changes in maximum keratometry (ΔK_{max}, diopters). Higher decrease in K_{max} (i.e., corneal flattening) is associated with greater increase of densitometry. Own representation, published in (55).

No correlation was observed between ΔcGSU-0-2A and preoperative ThCT (R = -0.022, p = 0.885) nor between ΔcGSU-0-2A and changes in thinnest corneal thickness (ΔThCT) (R = -0.27, p = 0.066). Age did not have any significant effect either on cGSU-0-2A at postoperative 12 months (R = 0.177, p = 0.233) or on ΔcGSU-0-2A (R = 0.097, p = 0.514). The analysis of the effect of preoperative values on corneal flattening revealed a significant negative correlation between ΔK_{max} and preoperative K_{max} readings (R = -0.302, p = 0.038), as shown in Figure 4. Although, no correlation has been found between ΔK_{max} and preoperative ThCT (R = 0.094, p = 0.53) nor between ΔK_{max} and ΔThCT (R = 0.147, p = 0.32).

DOI:10.14753/SE.2024.2880

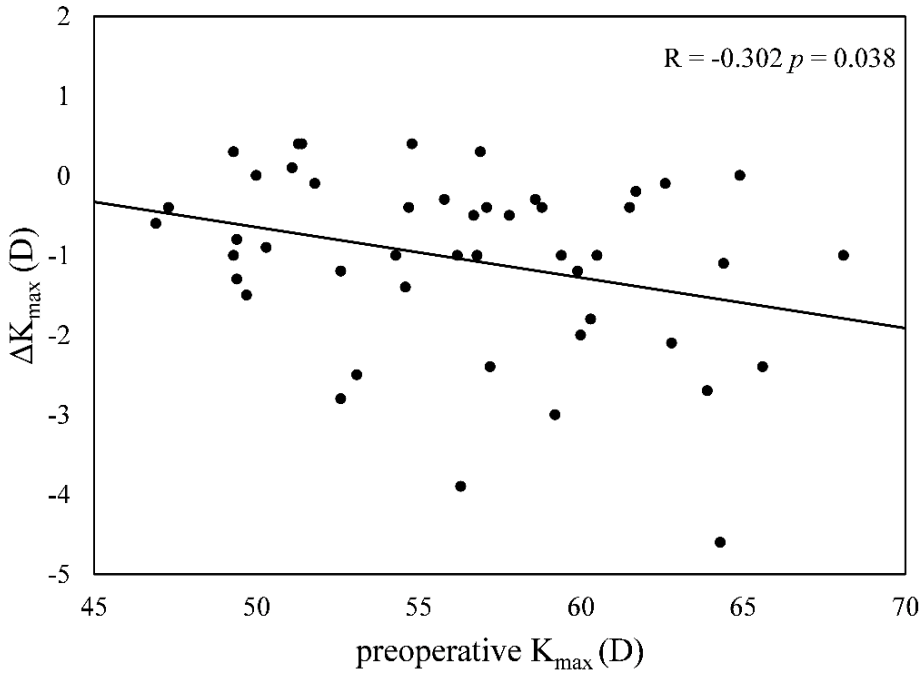

Figure 4. Changes in maximum keratometry (ΔK_{max}, diopters) at 12 months significantly correlated with preoperative maximum keratometry (K_{max}, diopters). Own representation, published in (55).

The result of GEE analysis indicated that postoperative densitometry (cGSU-0-2A) has a significant effect both on postoperative UCDVA (β coefficient = 0.006, p = 0.041) and postoperative BCDVA (β coefficient = 0.003, p = 0.039) after adjusting for the preoperative K_{max} readings (β coefficient = 0.026, p <0.001 and β coefficient = 0.018, p <0.001, respectively). These results are summarized in Table 3.

Table 3. Results of generalized estimating equations adjusted for preoperative K_{max} readings to determine the relationship between postoperative corneal haze (cGSU-0-2A, GSU/mm^3) and postoperative uncorrected and best corrected distance visual acuity (UCDVA and BCDVA, logMAR).

	UCDVA		BCDVA	
	β coefficient	p-value	β coefficient	p-value
cGSU-0-2A	0.006	0.041	0.003	0.039
K_{max}	0.026	<0.001	0.018	<0.001

4.2. Corneal microstructural alterations of patients with quiescent vernal keratoconjunctivitis

4.2.1. Patients' characteristics

In our study, 20 right eyes of 20 subjects with quiescent VKC (mean age of 12.45 ± 2.95 years, male:female ratio: 18:2) and 25 eyes of 25 healthy individuals as control (mean age of 12.64 ± 3.06 years, male:female ratio: 21:4) were involved. There were no significant differences between the VKC group and the control group regarding the age or gender distribution of the participants (p = 0.41 and p = 0.56, respectively). The average disease duration of VKC patients was 63.55 ± 25.94 months, while the average length of the quiescent phase was 5.25 ± 1.52 months. Prior to examinations, treatment-free periods ranged between 2 and 7 months. In the VKC group, personal history of atopy was recorded in 65% of cases. All included patients in the study were Caucasians (Table 4).

Table 4. Patients' characteristics. SD = standard deviation.

Variables	Vernal keratoconjunctivitis	Controls	p-value
Number	20	25	–
Age (mean ± SD, (range), years)	12.45 ± 2.95 (8–17)	12.64 ± 3.06 (6–18)	0.41
Gender (male:female)	18:2	21:4	0.56
Disease duration (mean ± SD, (range), months)	63.55 ± 25.94 (22–108)	–	–
Length of quiescent phase (mean ± SD, (range), months)	5.25 ± 1.52 (2–7)	–	–
Personal history of atopy (n, %)	13 (65%)	No	–
Family history of atopy (n, %)	10 (50%)	4 (16%)	–

4.2.2. Slit-lamp biomicroscopy and corneal alterations

At the time of the visit, all patients were free of ocular signs and symptoms, and upon slit-lamp biomicroscopy, no signs of conjunctival hyperemia, conjunctival secretion, corneal involvement, or limbal Trantas' dots were observed. The cohort was comprised of 3 eyes (15%) with grade 0; 9 eyes (45%) with grade 1; 2 eyes (10%) with grade 2 and 6 eyes (30%) with grade 3 according to the Bonini scale with a mean severity of tarsal papillary hypertrophy of 1.55 ± 1.09.

DOI:10.14753/SE.2024.2880

IVCM examination was successfully performed on all patients. The results showed that there were no significant differences in epithelial, keratocyte, and endothelial cell densities between the groups in all layers. Additionally, no significant difference could be detected in SBNP parameters between VKC and control groups (all *p*-values >0.05). LCs were identified in 80% of VKC patients and 76% of healthy subjects. In terms of the density of LCs, the mean LCD was 44.03 ± 32.86 cells/mm^2 in the VKC group, while the control group had a mean LCD of 20.68 ± 13.69 cells/mm^2; the difference was statistically significant (p = 0.005). Analysis of LCM showed that not only the LCD but also the proportion of LCs with longer processes was significantly increased in VKC patients (p <0.001) (Figure 5), as compared to healthy controls. Additionally, the LCF was significantly higher in the VKC group than in the control group (p <0.001). There were no leukocytes observed and no signs of keratocyte activation were found in any patients (Table 5).

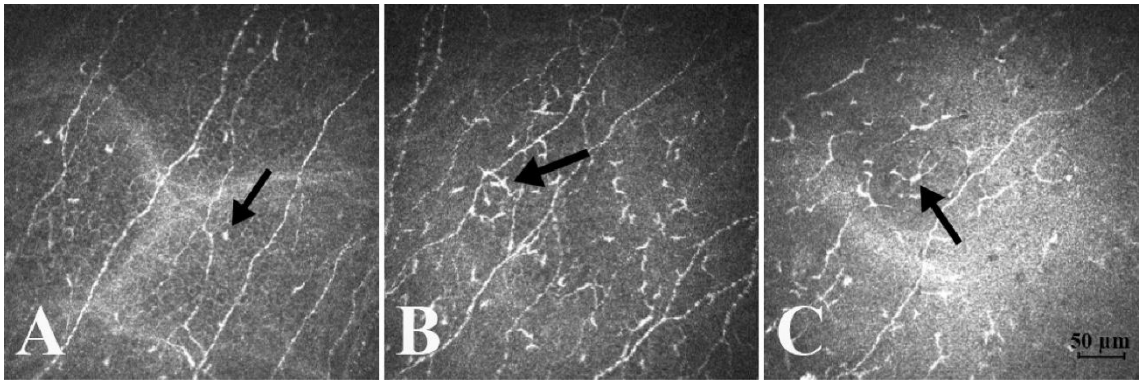

Figure 5. Representative confocal microscopy images of Langerhans cells (LCs) in the central cornea in a healthy normal patient (A) and in patients with vernal keratoconjunctivitis (VKC) (B, C). Note that some immature LCs (score 1 LC is indicated by the arrow) can be seen in the healthy cornea (A). Density of LCs is significantly larger in the VKC group than that in normal patients (B, C). LCs with small processes (arrow shows a score 2 LC) are presented in high density (B). LCs with long, interdigitating processes can be observed indicating mature form (arrow pointing at a score 3 LC) (C). Bar indicates 50 µm. Own images, published in (30).

Table 5. Results of in vivo corneal confocal microscopy. Data are displayed as mean ± standard deviation. CNFD = corneal nerve fiber density, CNFL = corneal nerve fiber length, CTBD = corneal nerve fiber total branch density, CNFW = corneal nerve fiber width. Significance level was set at p <0.05. *Statistically significant difference.

Variables	Vernal keratoconjunctivitis	Controls	p-value
Epithelium (cell/mm^2)			
Wing cell density	5230.2 ± 583.04	5521.5 ± 521.39	0.08
Basal cell density	8571.29 ± 710.72	8405.99 ± 756.53	0.46
Subbasal nerve plexus			
CNFD (number of fibers/mm^2)	16.16 ± 10.21	17.05 ± 8.48	0.65
CNFL (length of nerves mm/mm^2)	10.47 ± 2.99	12.39 ± 3.40	0.054
CTBD (number of branch points/mm^2)	31.276 ± 19.83	28.16 ± 19.43	0.44
CNFW (nerve fiber width mm/mm^2)	0.02 ± 0.002	0.02 ± 0.002	0.45
Tortuosity (grade)	0.65 ± 0.67	0.36 ± 0.57	0.17
Keratocyte cell density (cell/mm^2)			
Anterior stroma	813.8 ± 94.17	799.49 ± 124.77	0.67
Mid stroma	340.12 ± 44.65	350.56 ± 63.55	0.54
Posterior stroma	355.87 ± 64.68	346.41 ± 60.16	0.61
Endothelial cell density (cell/mm^2)	3116.03 ± 187.61	3215.19 ± 189.98	0.08
Leukocytes (cell/mm^2)			
Epithelium	Not observed		
Anterior stroma	Not observed		
Langerhans cell density (cell/mm^2)	44.03 ± 32.86	20.68 ± 13.69	0.005*
Langerhans cell morphology (score)	2.02 ± 0.61	1.04 ± 0.06	<0.001*
Langerhans cell field (μm^2)	1513.52 ± 830.85	154.44 ± 48.56	<0.001*
Keratocyte activation	Not observed		

4.2.3. Influencing factors of Langerhans cell morphology and cell density

The results of univariable GEE regression analysis showed that both the gender and the severity of papillary hypertrophy showed significant association with the LCD and with the LCF. However, age, personal or family history of atopy, length of the quiescent phase, and disease duration did not show any impact on it. After performing multivariable

regression analysis, only the severity of papillary hypertrophy remained significant (β-coefficient: 19.541, p <0.001 and β-coefficient: 595.255, p <0.001, respectively). Regarding the LCM, only the severity of papillary hypertrophy showed a significant impact (β-coefficient: 0.283, p <0.001) (Table 6).

Table 6. Regression analysis of the possible associated factors and their significance on the density and morphology of LCs. Significance level was set at p <0.05.

Variables	Langerhans cell density		Langerhans cell morphology		Langerhans cell field	
	β-coefficient	*p*-value	β-coefficient	*p*-value	β-coefficient	*p*-value
Age	3.136	0.12	-0.001	0.98	11.61	0.872
Gender	32.815	0.01	-0.260	0.08	-591.946	0.002
Personal history of atopy	22.982	0.08	0.259	0.48	635.589	0.55
Family history of atopy	6.833	0.63	-0.348	0.22	50.274	0.893
Length of quiescent phase	-4.956	0.19	-0.044	0.68	-23.787	0.819
Disease duration	0.368	0.14	0.007	0.08	3.271	0.63
Severity of papillary hypertrophy	19.541	<0.001	0.283	<0.001	595.255	<0.001

4.3. Corneal alterations in nephropathic cystinosis

4.3.1. Patients' characteristics

In our study, 12 eyes of 6 patients with nephropathic cystinosis were involved. The group included three children (2 boys and 1 girl, aged 8, 12, and 15 years) and three adults (2 men and 1 woman, aged 24, 26, and 36 years). The three patients under 18 years old were siblings. Despite the three adults and the oldest child having undergone renal transplantation previously, all involved subjects were in good general health, and the majority of them had good visual acuity. We observed diffuse crystal deposition throughout the entire cornea by slit-lamp biomicroscopy in each case (Figure 6). No detectable sign of corneal edema or scarring was observed in Patient 1–5. However,

in Patient 6, bilateral corneal scarring and plaque-like band keratopathy on the left cornea were found as a late-onset complication of corneal involvement, which explains her low visual acuity and high corneal thickness (674 μm). The mean CCT in the remained 11 eyes of 6 examined patients was 582.45 ± 25.91 μm. The clinical characteristics of the patients are summarized in Table 7.

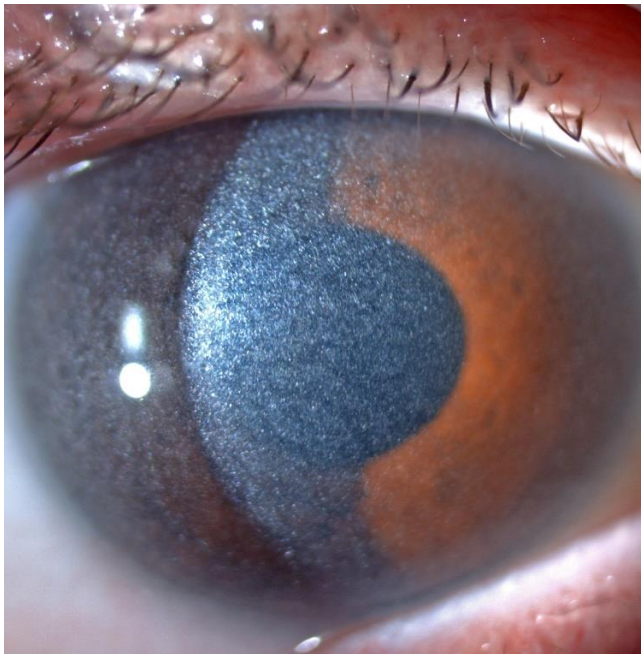

Figure 6. Representative slit-lamp image of a patient with nephropathic cystinosis with diffuse crystal deposition in the cornea.

Table 7. Clinical characteristics of patients with nephropathic cystinosis. BCDVA = best corrected distance visual acuity (logMAR).

Patient	Age (years)	Gender	Renal transplantation	Eye	BCDVA (logMAR)
1	8	male	no	right	0.0
				left	0.0
2	12	male	no	right	0.0
				left	0.0
3	15	female	yes	right	0.0
				left	0.0
4	24	male	yes	right	0.0
				left	0.0
5	26	male	yes	right	0.0
				left	0.0
6	36	female	yes	right	1.0
				left	1.0

4.3.2. Corneal architecture, characteristics of crystal arrangement and age-related alterations

AS-OCT images revealed the deposition of hyperreflective crystals extending from limbus to limbus in all patients. No DCD measurement was performed in the case of Patient 6 due to the corneal scarring appearing as a hyperreflective area on AS-OCT scans, exact differentiation of hyperreflective crystals from scarred areas was not feasible. AS-OCT scans demonstrated that the crystal deposits are located deeper with increasing age (Figure 7A–E). In younger children, mainly the anterior stroma is involved (Figure 7A–B), whereas in the oldest child (15 years old) the majority of the deposits affected both the anterior and middle stroma as well (Figure 7C). In pediatric patients, no crystals were observed in the posterior parts. However, in adults, the crystal deposition mainly involved the posterior two-thirds of the corneal stroma (Figure 7D–E).

DOI:10.14753/SE.2024.2880

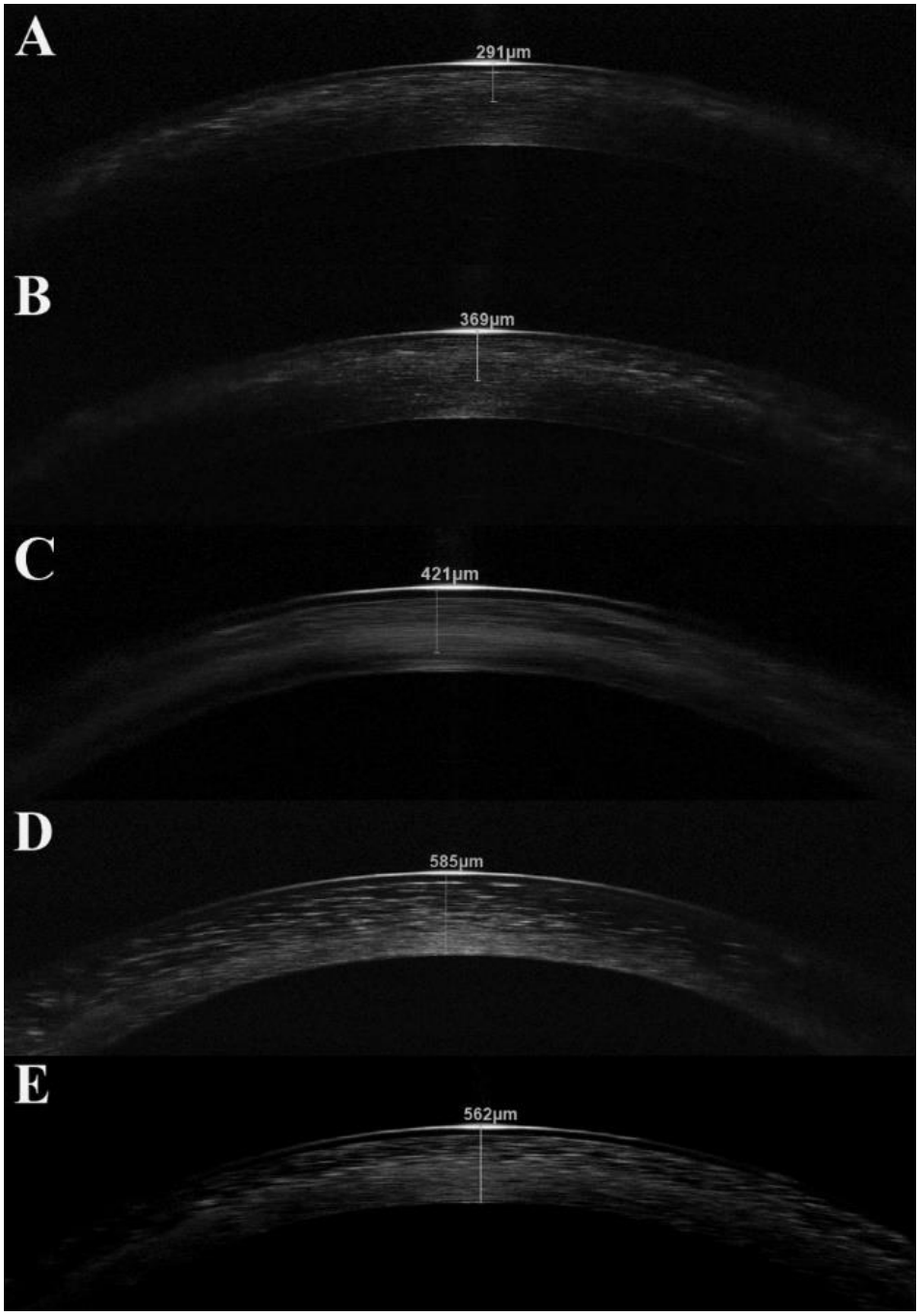

Figure 7. Anterior segment optical coherence tomography scans of the cornea in nephropathic cystinosis in ascending order with age. In children, the anterior stroma is predominantly involved in crystal deposition (A–C). In Patient 3, the crystal location is deeper, but the posterior stroma is still not affected (C). On the contrary, in adults the crystals are mostly located in the posterior stroma (D–E). Own images, published in (56).

In children, the mean DCD was 353.17 ± 49.23 μm, while in adults it was 555.75 ± 25.27 μm. The DCD values were plotted against the age of the subjects as shown in Figure 8. According to the graph, the two eyes are showing similar values, and a tendency for the localization of the age-related crystal deposition can be observed.

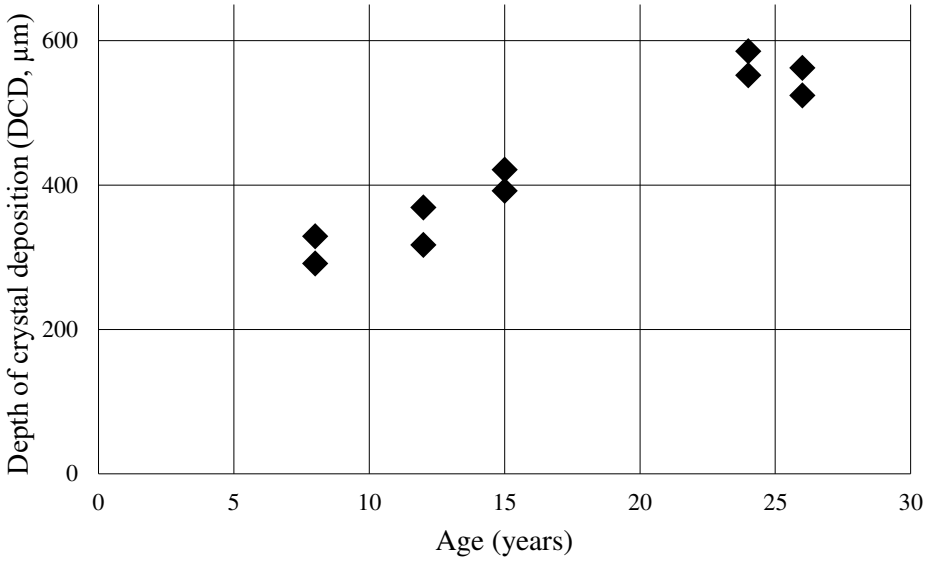

Figure 8. Depth of crystal deposition (DCD) measured on anterior segment optical coherence tomography images. DCD values show an increasing tendency with age. In all patients available for the measurement the DCD values were symmetrical in both eyes that is observable on the distribution of the plot. Own representation, published in (56).

Concerning the IVCM images, the crystals appeared as hyperreflective, sharply defined, elongated structures with varying sizes and shapes. The crystals were randomly oriented without any differentiation and could be observed throughout the full thickness of the cornea with the exception of the endothelium. Regarding the epithelial layer, short and thin deposits were seen extracellularly in nine eyes of five patients. The mean CD of the epithelium was 1.47 ± 1.17 (median: 1.5; interquartile range (IQR): 0.3–2.4). All examined patients had crystals in the entire corneal stroma. Narrow and needle-shaped deposits were found mainly in the anterior stroma in the three involved children. Keratocytes could not be detected in these images as shown in Figure 9A. In children, the mean CD in the anterior stroma was 3.37 ± 0.34 (median: 3.4; IQR: 3.25–3.55). In adults, aggregated, thick and long crystals were observed in the anterior stroma surrounded by homogeneous, acellular hyporeflective regions (Figure 9C). The mean CD in the anterior

stroma of adults was 1.23 ± 0.23 (median: 1.2; IQR: 1.05–1.35). The CD in the anterior stroma was found to be greater in younger patients compared to older subjects (Figure 10). Analysis of IVCM images of the posterior corneal stroma of children showed that the crystals were narrower, keratocyte nuclei were seen clearly, and normal stromal structure was detected with a mean CD of 0.76 ± 0.49 (median: 0.7; IQR: 0.4–1.15) (Figure 9B). It was not possible to determine whether the crystals are intra- or extracellularly-located since the cell borders of keratocytes were not visible. In adults, the highest crystal density was found in the posterior stroma with a mean CD of 3.63 ± 0.29 (median: 3.7; IQR: 3.45–3.8) (Figure 10). Only the crystals could be detected in this layer, and no other cells (Figure 9D). The endothelium was spared and had an intact structure in each case. Data of DCD and CD values in different corneal layers are summarized in Table 8.

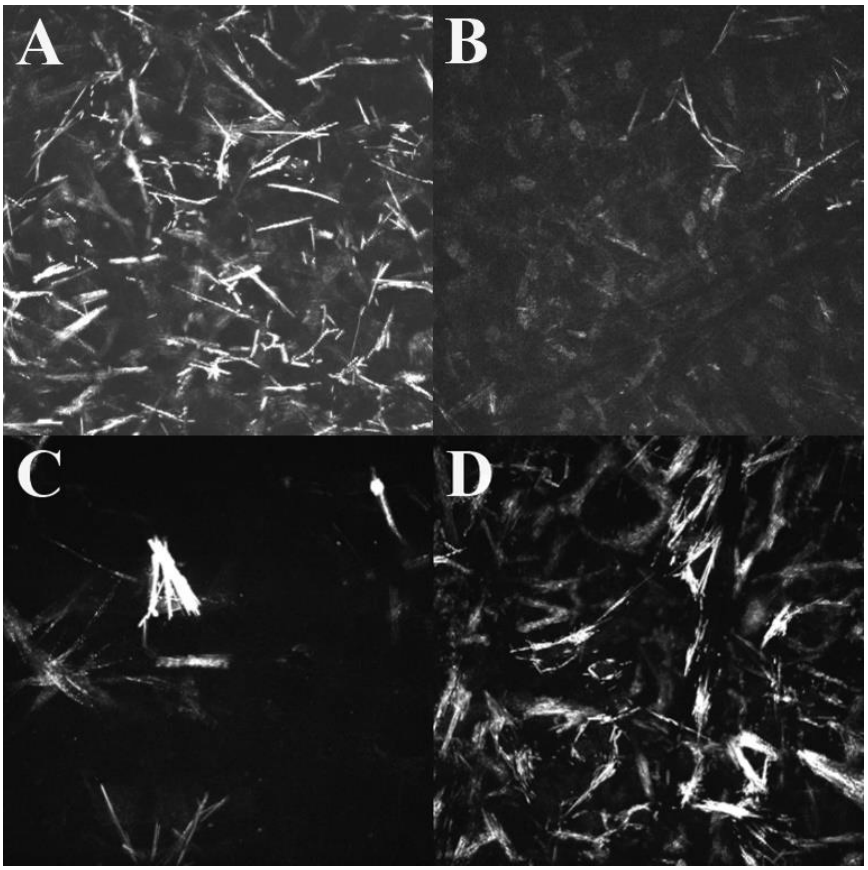

Figure 9. In vivo confocal microscopy images showing different stromal arrangement of the deposits. In children, many deposits are in the anterior stroma (A). The posterior stroma is intact in children: few crystals and many keratocytes are visible (B). On the contrary, few crystals are aggregated in the anterior stroma of adults (C), whereas their posterior stroma has high crystal density (D). Own images, published in (56).

DOI:10.14753/SE.2024.2880

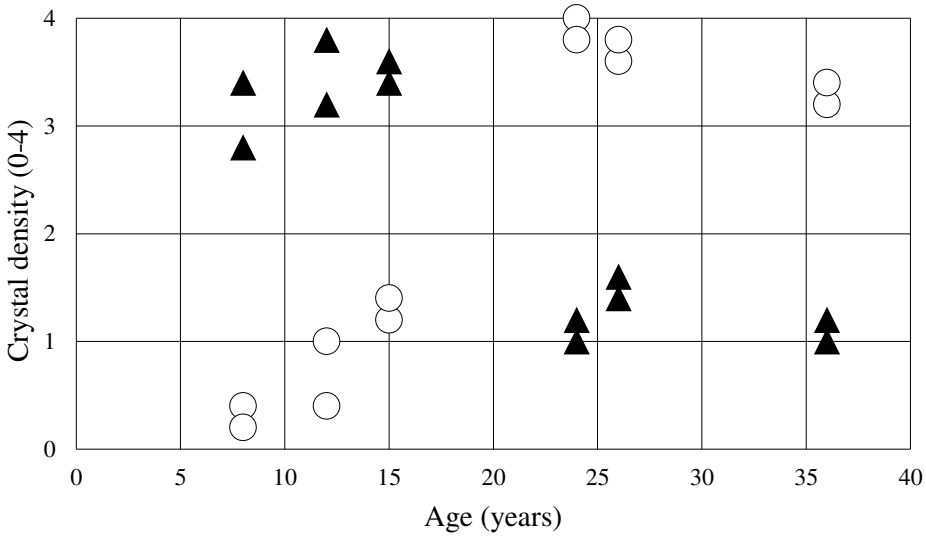

Figure 10. Crystal density (CD) of anterior and posterior stroma. Semiquantitative analysis of deposits showed higher density in the anterior stroma in children and higher density in the posterior stroma in adults. ▲ CD in the anterior stroma; ○ CD in the posterior stroma. Own representation, published in (56).

Table 8. Central corneal thickness (CCT) in μm, depth of crystal deposition (DCD) in μm and crystal density (CD) values in the study subjects. The CD values were derived from five measurements in the given area.

Patient	Eye	CCT	DCD	CD			
				Epithelium	Anterior stroma	Posterior stroma	Endothelium
1	right	613	329	1.6	3.4	0.4	0.0
	left	627	291	1.2	2.8	0.2	0.0
2	right	611	317	1.4	3.2	1.0	0.0
	left	583	369	2.4	3.8	0.4	0.0
3	right	582	392	3.2	3.4	1.2	0.0
	left	550	421	2.4	3.6	1.4	0.0
4	right	564	552	0.0	1.2	4.0	0.0
	left	554	585	0.4	1.0	3.8	0.0
5	right	555	562	2.0	1.4	3.6	0.0
	left	587	524	3.0	1.6	3.8	0.0
6	right	581	-	0.0	1.0	3.2	0.0
	left	674	-	0.0	1.2	3.4	0.0

DOI:10.14753/SE.2024.2880

The majority of the corneal crystals were oblong and needle-shaped according to the IVCM recordings. Interestingly, in two patients we also found hexagonal crystals. In Patient 1 (8 years old) only a few of these crystals could be observed, and they were located in the anterior stroma (Figure 11A). In Patient 5 (26 years old), several hexagonal crystals of various sizes were detected in both the anterior and posterior stroma (Figure 11B).

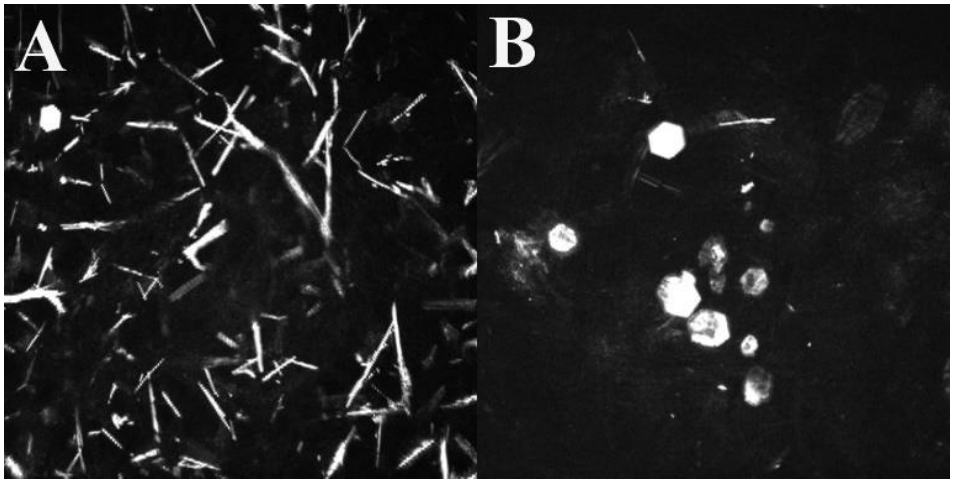

Figure 11. Hexagonal crystals. One hexagonal crystal is visible on the in vivo confocal microscopy image of a child (A). Some hexagonal crystals in adult (B). Own images, published in (56).

5. Discussion

5.1. Effects of conventional cross-linking therapy in progressive keratoconus

Regarding the investigation of the effects of CXL therapy in patients with keratoconus, we reported the classical corneal optical densitometry changes during 1-year follow-up and the impact of keratometric and pachymetric values on haze formation and corneal flattening.

According to our results, an initial impairment of UCDVA and BCDVA in the first postoperative month could be detected. Subsequentially, this worsening was followed by improvement, although one year after the treatment, it was not statistically significant compared to the baseline value. A congruent trend could be demonstrated in the changes of K_{mean} and K_{max} readings, with a peak value at 1 month but with a following significant flattening 12 months later. The densitometry values reached their peak between the first and the third months postoperatively but they began to decrease thereafter. We suppose that our results are in line with the previously demonstrated CXL-related cellular changes, i.e., keratocyte loss due to apoptosis and development of edematous and hyperreflective extracellular stroma (11). Presumably, during the early postoperative months, the CXL-induced stromal alterations cause greater keratometry and densitometry values and impairment of visual acuity.

The comprehensive analysis of the optical densitometry values of the cornea showed increased values after CXL in the three central rings (0–2 mm, 2–6 mm, 6–10 mm). Changes in densitometry values could be observed in the anterior and center layers, while the posterior layer was spared in all regions. The explanation for this phenomenon is that CXL primarily exerts its effects within 300 µm depth in the corneal stroma (57, 58). In previous clinical trials which used slit-lamp biomicroscope for haze assessment, it has been shown that corneal haze typically lasts less than 12 months (59, 60). The first slit-lamp-based grading of postoperative haze evaluation was first described by Fantes *et al.* on a scale from 0 to 4 (61). However, this method is not suitable for the detection of very slight changes in haze levels, thus it is not accurate enough for statistical purposes. Furthermore, the application of this grading is a subjective method, and it has inherent limitations regarding intra- and interobserver repeatability and reproducibility (62). The Pentacam HR Scheimpflug camera with the add-on densitometry software may

ensure corneal haze assessment in greater detail. In our study, it has been demonstrated that the densitometry values remained elevated in the anterior, center and total layers of 0–2 mm and of 2–6 mm rings, and in the center and total layer of 6–10 mm ring compared to the preoperative values. The observed pattern closely resembles the results of previous studies in which Scheimpflug imaging was used for densitometry analysis (12, 14, 44, 63). This suggests that persistent cellular alterations in the central regions of the cornea may be observed at least one year after CXL therapy.

The available literature differs in terms of which corneal region is primarily affected by CXL. The majority of the studies reported that the most significant densitometry change is presented in the anterior layer (14, 44), however, the main involvement of the center layer has also been reported by some authors (12). The reason for this might be that the thickness of the center corneal layer differs in each subject and it is not specified in exact μm in Cornea Densito software. Hence, in corneas with higher thickness, the values obtained from the center layer may represent measurements taken from a thicker layer, which potentially influences the assessed results. Additionally, the different surface areas of examined rings may also influence the results (44). Therefore, a new additional calculation for densitometry data was used according to Nemeth *et al*. (44). With this calculation, we got surface area- and thickness-corrected densitometry values, which allowed us the possibility to evaluate values independently of the individual corneal thickness or different surface areas of examined rings. By utilizing the corrected densitometry data, our evaluation indicated that change in densitometry in the anterior layer of 0–2 mm ring could be observed as the most characteristic parameter of corneal densitometry changes.

The majority of the available studies evaluated the relationship between CXL-related corneal haze and postoperative outcomes (12-14), although the impact of preoperative parameters on the postoperative amount of haze has remained undefined thus far. Significantly higher densitometry in eyes with a higher decrease in keratometry was reported by Pircher *et al*. but without clarification of the exact correlation between them (14). In our analysis, we evaluated the influence of the preoperative parameters, specifically ThCT and K_{max}, which correlate with the severity of keratoconus on corneal haze formation and flattening. Changes in haze and in keratometry significantly correlated with preoperative K_{max}, while no other preoperative factors showed significant

correlation. Recent data highlighted the importance of preoperative keratometry as a prognostic indicator for determining the extent of topographic flattening after CXL (64-67). Our results also provided evidence that in corneas with higher preoperative keratometry readings, a greater flattening might be expected. Ultrastructural examinations of corneas with keratoconus revealed a high proportion of loosely packed and randomly oriented collagen fibrils (67). Notably, the amount of structural changes differs as the stage of the disease progresses (68). In the case of advanced keratoconus, the cross-linking effect may penetrate relatively deeper, resulting in a larger proportion of stroma becoming crosslinked, which may lead to a higher extent of haze. This phenomenon may explain the more pronounced haze formation in patients with higher keratometry readings, and suggest that increased densitometry values may be indicative of the effectiveness of CXL in terms of corneal flattening and stiffening.

The age of patients may influence corneal transparency, as shown through Pentacam imaging in normal corneas (69). Thus, we incorporated the patients' age in our analysis, to assess whether it has any impact on corneal haze formation. It also has been reported that the severity of keratoconus influences the corneal clarity: in cases of more advanced keratoconus, higher densitometry values may be observed due to the increasing corneal damage (70). Studies investigating corneal haze formation after CXL treatment vary regarding the age of involved patients. Some reports strictly include adults over 18 years (12, 14, 71, 72), while others involved patients under 18 years as well (44, 73, 74). However, the presented tendencies in densitometry changes are similar. According to the results of a recent report, significantly higher postoperative corneal haze formation can be expected after CXL therapy compared to adults in juvenile keratoconus (75). Our results suggest that the postoperative densitometry changes after CXL in adults are more closely related to the severity of keratoconus rather than the age of patients, which is in agreement with the available literature (12-14, 70).

There are contradictory results in terms of visual outcomes after conventional CXL therapy. Some studies reported significant improvement in BCDVA (12, 76, 77), however, there are others that did not support this result (14, 63, 66). Recent data suggest that preoperative keratometry readings have a significant impact on postoperative visual acuity, with patients having higher preoperative keratometry presenting greater improvement in BCDVA (78-80). Previous results suggest that CXL-induced corneal

haze does not affect high-contrast visual acuity (14, 63). In our study, the decrease in the keratometry values was not accompanied by an improvement in visual acuity. Therefore, we evaluated the effect of densitometry values on UCDVA and BCDVA using generalized estimating equations. We kept the keratometry readings in the model to eliminate the effect of corneal irregularity characterized by higher keratometry values. According to this analysis, we showed that increased densitometry values negatively affected the visual acuity 12 months after CXL. In our cohort, although significant corneal flattening was found, there was no significant improvement neither in UCDVA nor in BCDVA at the end of the follow-up period. Based on these results, we can conclude that the improvement in visual acuity associated with the decrease in keratometric values may be impeded by haze formation, thus limiting the effectiveness of the treatment in terms of the improvement in vision through corneal flattening.

Currently, there is no widely accepted protocol concerning the type of topical corticosteroids used in the postoperative period after CXL. According to the recent literature, fluorometholone is the most frequently used topical corticosteroid after CXL for minimizing haze formation (13, 44, 59, 81). Although the role of corticosteroids in the treatment of postoperative corneal haze is still questionable, the effect of different types of topical corticosteroids on haze formation might be different (82, 83). Haze is related to the stromal wound healing response, thus, theoretically, the possibility arises that a more pronounced haze develops when the inflammatory reaction is treated with a less potent anti-inflammatory agent (e.g. fluorometholone). A recent study has shown that keratoconic eyes may have a predisposition for developing steroid-induced ocular hypertension when treated with topical dexamethasone after CXL (84). However, there is no currently available data regarding the intraocular changes when using low-potency corticosteroids, such as fluorometholone, after CXL. Theoretically, in more advanced keratoconus, where more significant haze formation is expected, the application of potent topical corticosteroids may be considered with close monitoring of the intraocular pressure. Further research is required to investigate the impact of various topical corticosteroids on haze formation following CXL.

Some limitations of our study must be mentioned. Although the follow-up period in our cohort was 12 months, it is possible that the degree of corneal haze may change beyond this time frame. This may impact the generalizability of our results to those, for

whom several years elapsed since the treatment. Furthermore, previous studies showed that the repeatability of densitometry measurement was low in CXL-treated corneas (85). Therefore, to obtain more exact results, it would have been preferable to use the average value of three measurements at each follow-up visit, but this was limited by the retrospective manner of our analysis. In addition, evaluating data of separated groups according to the severity of keratoconus might have influenced our final results. Estimating possible haze formation according to different stages of keratoconus based on a detailed classification system (such as the ABCD grading system) might be useful for clinicians in predicting postoperative results more accurately.

5.2. Corneal microstructural alterations of patients with quiescent vernal keratoconjunctivitis

Recent data suggest that due to the chronic inflammation and persistent mechanical trauma, several abnormalities of the ocular surface can be developed in long term in VKC patients. Interestingly, various subclinical alterations were reported even in paucisymptomatic cases, such as decreased corneal and lens transparency, an increase of posterior corneal astigmatism, impaired tear film stability, and greater levels of proinflammatory proteins in the tear film (23-25, 86). In our research, we investigated the corneal morphology in patients with quiescent VKC compared to healthy controls to determine whether subclinical morphological alterations may be observed in the cornea via IVCM. In addition, the morphology and density of LCs, as well as their associated factors were analysed.

It has been shown previously that the local inflamed milieu in active VKC contributes to the development of microstructural changes mainly in the anterior corneal parts. These include the reduced cell number of basal epithelium and anterior stromal keratocytes, and a higher number of leukocytes and activated keratocytes (22, 26, 28). The impaired structure of the SBNP was also demonstrated, consisting of lower density and length of fibers, decreased number of branches, and higher grade of tortuosity (28). In our study, we could not observe any differences in asymptomatic VKC compared to healthy subjects neither in terms of cell densities of corneal layers nor regarding the morphology of SBNP. Our findings indicate that during the quiescent phase, the corneal

microstructural abnormalities appear to recover without resulting in any permanent morphological lesion.

Corneal LCs have an essential role in the activation of naive T-cells and in determining the type of immune response. This is accomplished by affecting the cytokine environment of activated T-cells in allergic reactions (87, 88). Corneal LCs can be observed in a healthy cornea as well, and their phenotype depends on their maturity. Immature cells typically have large cell bodies and short or absent processes. Conversely, smaller cell bodies with longer dendrites are related to the maturation process (3). Upon different stimuli, immature LCs can capture antigens and undergo a transformation into a mature phenotype to present antigens to T-cells. This process includes the migration of LCs from the limbus to the central cornea (48, 89-91). IVCM is a valuable tool in the imaging of corneal LCs, and the distinguishment of mature and immature forms from other structures can be easily performed with it (92). In some recent studies, a higher percentage of LCs in eyes with VKC compared to healthy controls was observed during the active phase of the disease (27, 90). Analysing the asymptomatic corneas of VKC subjects in our study showed that the proportion of patients with detectable LCs was similar in both the VKC group (80%) and in healthy controls (76%). However, the density of LCs in the central cornea was significantly higher in VKC compared to controls. Furthermore, LCs with elongated dendrites were also presented, which indicates a maturation process and potential activity. Measurement of LCF, which is related to the maturity of the cells (52), has revealed that the LCs of patients with VKC have enlarged field areas compared to the LCs of healthy subjects. These novel findings indicate that certain triggering factors exist even in the inactive phase of VKC, which contributes to maintaining an active inflammatory process in the cornea, thus, increasing the density of resident LCs and stimulating the maturation process in the absence of clinically manifest ocular inflammation.

The cobblestone-like formation of giant papillae is a characteristic symptom of VKC. The fibrovascular proliferation of the conjunctival stroma, hence the formation of giant papillae is facilitated by Th2-type cytokines and various growth factors such as TGF-β, bFGF, and PDGF (17). Typically, active local inflammation results in the enlargement of the papillae up to 5 mm in size, mucoid discharge accumulation on the top, and the development of hyperemia. Although giant papillae are commonly associated with active

local inflammation, the tissue remodeling changes can lead to the permanent presence of papillary hypertrophy. Thus, they may be present even in the off-season of the disease, without any local signs of disease activity (15). It has been suggested before that chronic disturbance of the ocular surface can lead to a shift toward the activation of an inflammatory response, which involves the recruitment of LCs (92). A previous study has indicated that patients with quiescent VKC have reduced corneal optical transparency compared to healthy individuals, suggesting subclinical alteration of corneal microstructure. These findings have been attributed to the assumption that recurrent microtrauma due to the eye-rubbing and protruding tarsal papillae may be the underlying cause (23). Our analysis demonstrated that the degree of papillary hypertrophy closely is correlated with the LCD, LCM, and LCF. Specifically, the more severe papillary hypertrophy was associated with higher density and higher maturation stage of these cells. Presumably, giant papillae play a role in producing persistent mechanical irritation of the corneal surface, which may, in turn, facilitate the enrollment and maturation of LCs. Thus, for patients with persistent papillary hypertrophy, the use of topical treatment (e.g., lubricants) may be advisable even during the inactive phase of the disease. However, further longitudinal studies are required to clarify the clinical role and exact relationship between the increased activity of LCs and long-term alterations of the ocular surface or of the cornea.

There might be some other unknown triggering factors, which may contribute to the increased activity of LCs. Subclinical tear film dysfunction in patients with quiescent VKC has been reported by Villani *et al.* (24). Inadequate hydration of the ocular surface leads to the induction of proinflammatory cytokines, including IL-1, IL-6, IL-8, and TNF-α (93). It has been confirmed that these cytokines may induce the recruitment and maturation of LCs implying that abnormalities in the tear film stability may serve as a potential trigger for LCs maturation (94). Previous studies demonstrated that increased density and activity of LCs can be observed in the central cornea in patients with systemic diseases characterized by chronic inflammation, even in the absence of ocular symptoms (49-51). Thus, we hypothesized that atopy may affect the LC population of the cornea, but we could not confirm this in our analysis due to the lack of statistical significance.

Our study was focused on identifying morphological changes, although simultaneous examination of the tear protein profile and tear film function in correlation with the

alterations in LCs could have provided additional insight into the connection between the LC presence and ocular surface disturbances. Examination of the limbal area with IVCM could have yielded additional data on morphological changes, as immunological processes in the limbus also have a significant role in the pathophysiology of the ocular surface (95). Although the rare occurrence of VKC might have imposed limitations on the study sample size, our results provide new insights into the course of VKC and present an accurate characterization of the corneal alterations associated with this ocular surface disease.

5.3. Corneal alterations in nephropathic cystinosis

To the best of our knowledge, our study is the first in the literature that investigated the properties of cystine crystal localization in cystinosis in relation to age using both IVCM and AS-OCT imaging. In our study, we reported the characteristics of the appearance of cystine crystals analysing the records of 12 eyes of 6 patients with nephropathic cystinosis. In the case of 5 out of 6 patients, we observed epithelial involvement, consistent with the findings of several previous studies (6, 32, 36, 38). Notably, in all cases in our cohort, the endothelium was spared, although previous data indicate that endothelial involvement may also occur (40, 96).

There are contradictory data in the available literature concerning the stromal pattern of corneal crystal deposition in cystinosis. While most of the studies describe that the majority of the deposits are located in either the anterior or posterior stroma (36, 39), there are some case reports, which demonstrate the main involvement of the middle layer (35, 38). It has been previously confirmed by histopathological and clinical studies that crystal deposition begins at the anterior and peripheral part of the cornea and gradually spreads posteriorly and centrally with aging (40, 97, 98). Our findings were consistent with these previous reports, i.e., in the three children, crystal deposition was primarily observed in the anterior stroma, whereas in adults, the posterior stroma had the highest crystal density. We also demonstrated that despite this localization trend, crystal deposition could be observed in full stromal thickness in all ages. According to our data, both AS-OCT and IVCM confirmed that accumulation of the crystal deposits has an increasing tendency in the posterior stroma with aging.

Our findings suggest that the cystine crystal deposition might cause alterations in the keratocyte population. The IVCM images revealed keratocyte dropout in the regions where significant crystal deposition was observed. Specifically, in children with cystinosis, no loss of keratocytes was found in the posterior stromal regions, whereas in adults, keratocytes were absent throughout the full corneal thickness. In vitro studies reported progressive keratocyte disruption, keratocyte loss in corneal cystinosis, and a higher apoptotic rate in nephropathic cystinotic fibroblasts (99, 100). These findings are consistent with our in vivo findings in terms of the absence of keratocytes in affected areas.

Interestingly, we observed hexagonal-shaped crystals in two patients located in the stroma. Previous histopathological and IVCM studies reported that the cystine crystals are typically needle-shaped in the cornea (39, 40, 101, 102), while they might be hexagonal or polygonal in other organs (103). The role of stromal collagen in needle-shaped crystallization was emphasized by Dixon *et al*. (104). According to their results, due to the charge-charge interactions between the anionic collagen fibrils and cationic cystine, cystine amino acid is bound to the surface of collagen. The tightly located collagen lamellae inhibit the three-dimensional growth, hence the polygonal forming of crystals (104). The presence of hexagonal deposits in our patients indicates that the regular, tightly packed structure of the collagen lamellae in the cornea may be disrupted, potentially allowing for the growth of the crystals not only in parallel but in vector direction as well.

Several age-related corneal complications have been reported in nephropathic cystinosis including band keratopathy, corneal neovascularization, and scarring, although the exact cause of these complications remained unclear (105, 106). So far, we are not aware of any association between the changes in stromal microarchitecture and the risk of developing any late-onset corneal complication in nephropathic cystinosis. However, further studies are required to elucidate whether the crystal location and stromal alterations have a role in the development of late-onset complications.

All involved subjects underwent AS-OCT examination in our analysis, which could be performed easily due to its noninvasive manner even in young patients (see the 8-year-old subject in our study). Cross-sectional scans ensure an easy determination of the most affected parts of the cornea, although neither epithelial nor endothelial

involvement could be assessed using this imaging method due to its lower resolution. Additionally, corneal scarring made impossible the exact DCD measurement, hence crystals are not visible in the area of the scar. According to our findings, due to its higher magnification and higher resolution, IVCM is more precise than AS-OCT for the assessment of cystine crystals. With this method it is possible to evaluate the epithelial and endothelial involvement. Additionally, this technique ensured the imaging of deposits in regions of corneal scarring as well. Moreover, we found deposits throughout the entire corneal thickness in all patients, even in those who had only anterior corneal involvement according to the AS-OCT images. Despite the precise assessment of corneal involvement, IVCM might be not suitable for patients who have difficulties with contact examination. In several previous studies, the Gahl-score was utilized for the assessment of corneal involvement, which is a set of slit-lamp photographs of corneas containing cystine crystals at different densities (37). Later, a new IVCM scoring system has been published by Labbé *et al*., which provides a more accurate evaluation of crystal density and enables the comparative evaluation of crystal density in different layers of the cornea (36).

Theoretically, it cannot be ruled out that the continuous administration of the regularly applied eye drop in patients with cystinosis, i.e., the topical CH drop may influence the corneal crystal arrangement. Currently, there are no available studies about the lifelong effects of topical CH drops on the arrangement of deposits and about its impact on age-dependent changes. The diffusion of hydrophilic CH through the lipophilic epithelium is low (107). The aqueous formulation of the commonly used CH drops results in a short corneal contact time, hence, the dose regimen is frequent up to 12 times per day (108). These factors impose a significant burden on patients and may lead to poor adherence to the suggested therapy (108). The efficacy of 0.1% CH drops in reducing crystal density is low even in anterior stroma (109). These limits make it less likely that topical CH would have a profound impact on crystal arrangement at full corneal depth.

The potential limitation of our study could be the low number of cases. However, the rarity of nephropathic cystinosis could not make it possible to involve more patients. The available data about the assessment of crystal localization using IVCM and/or AS-OCT is limited (35, 36, 38, 39). Considering this limitation, we believe that our study provides important findings and shows clearly the inherent tendency between the age and stromal density of the deposited crystals. We attempted to divide the patients into two

subgroups to represent the differences between younger and older ages. However, due to the low sample size of our cohort, we were unable to statistically evaluate the average values of these groups. Our study was not primarily concerned with the distinction between children and adults in terms of the deposition of crystals but showed the relationship between the localization of the crystals and the age of the patients. Due to the rare occurrence of cystinosis, recruiting a large cohort of these patients of different ages is challenging, but it could provide precise statistical evaluation, which may confirm our results.

DOI:10.14753/SE.2024.2880

6. Conclusions

According to our results, the followings can be concluded:

The microstructural corneal changes after conventional epi-off CXL therapy for progressive keratoconus can be detected even one year after the surgery with the optical densitometry module of the Pentacam HR Scheimpflug camera. Our results showed that the greater preoperative K_{max} values are associated with a greater increase in corneal densitometry and a greater corneal flattening effect postoperatively. Thus, CXL treatment has a greater regularizing effect in more advanced keratoconus, however it is followed by a more prominent haze formation. Additionally, we demonstrated that despite CXL therapy being effective in increasing the stability of corneal ectasia and reducing keratometry, visual acuity may be limited by the loss of transparency.

Regarding the corneal microstructure in patients with quiescent VKC compared to healthy subjects, no morphological changes were presented in terms of cell densities of different corneal layers or SBNP morphology investigated via IVCM. However, increased density and maturation stage of LCs could be revealed in VKC patients in relation to the severity of tarsal hypertrophy. According to the sustained presence of LCs in elevated density and in a larger proportion of mature phenotype, chronic, ongoing activation of immune response and the sustained inflammatory process can be indicated, even in the absence of clinically manifested symptoms.

In nephropathic cystinosis, both AS-OCT and IVCM appear to be valuable imaging methods for the detection of the morphological characteristics of cystine crystal deposition and corneal structural changes. We demonstrated that there is a tendency for age-related distribution of crystal deposition with concomitant loss of keratocytes. Our results also showed that, in addition to needle-shaped crystals, hexagonal crystals may occur in the stroma in some cases, which may indicate a disruption of the structure of collagen lamellae.

DOI:10.14753/SE.2024.2880

7. Summary

The contemporary anterior segment-imaging techniques allow us the quantitative evaluation of certain parameters of corneal structure and may broaden our knowledge of the pathophysiology of various diseases. In our studies, we used various imaging methods to investigate the corneal microstructure from different aspects and to visualize characteristic alterations in different clinical conditions.

First, a retrospective analysis was performed on 47 eyes of 47 patients with progressive keratoconus using the Pentacam HR Scheimpflug camera before and 1, 3, 6, and 12 months after CXL therapy. The study was focused on the changes in corneal densitometry values, which are indicative of the natural course of the most characteristic CXL-related structural alteration, i.e., the stromal haze formation. Besides, the changes in visual acuity, pachymetry keratometry, and the effects of densitometry values on visual outcomes were analysed. Our findings indicated that in more advanced keratoconus more significant corneal flattening parallel with haze formation can be observed. Moreover, despite the significant reduction of keratometry, postoperative haze may limit the final visual acuity.

In the second study, 20 patients with quiescent VKC and 25 controls were compared in terms of cell density of different corneal layers and morphology of SBNP using IVCM in a cross-sectional manner. The main aim of this study was to assess whether any signs of an ongoing inflammatory process or of long-term structural alteration can be observed. Our data showed that in quiescent VKC, LCD, LCM, and LCF were increased, and they were associated with the severity of papillary hypertrophy. Alterations of Langerhans cells indicate a subclinical inflammatory process without ocular symptoms.

In our third study, we analysed the characteristics of crystal arrangement in different corneal layers and assessed morphological changes in relation to age in three children and three adults who had nephropathic cystinosis using IVCM and AS-OCT in a cross-sectional manner. Our results confirmed an age-related pattern of crystal deposition. In children, crystals tend to locate anteriorly, while in adults, deposits are found posteriorly in the corneal stroma.

Our studies conducted on CXL-treated keratoconus, quiescent VKC, and nephropathic cystinosis revealed novel findings regarding corneal microstructural alterations and may contribute to a better understanding of the course of these conditions.

8. References

1. Ambrosio R, Jr., Valbon BF, Faria-Correia F, Ramos I, Luz A. Scheimpflug imaging for laser refractive surgery. Curr Opin Ophthalmol. 2013;24(4):310-20.

2. Spadea L, Maraone G, Verboschi F, Vingolo EM, Tognetto D. Effect of corneal light scatter on vision: a review of the literature. Int J Ophthalmol. 2016;9(3):459-64.

3. Guthoff RF, Bauduin C, Stave J. Atlas of confocal laser scanning in-vivo microscopy in ophthalmology. Springer-Verlag Berlin; Heidelberg; 2006, 3 p.

4. Patel DV, McGhee CN. Contemporary in vivo confocal microscopy of the living human cornea using white light and laser scanning techniques: a major review. Clin Exp Ophthalmol. 2007;35(1):71-88.

5. Petroll WM, Robertson DM. In Vivo Confocal Microscopy of the Cornea: New Developments in Image Acquisition, Reconstruction, and Analysis Using the HRT-Rostock Corneal Module. Ocul Surf. 2015;13(3):187-203.

6. Liang H, Baudouin C, Tahiri Joutei Hassani R, Brignole-Baudouin F, Labbe A. Photophobia and corneal crystal density in nephropathic cystinosis: an in vivo confocal microscopy and anterior-segment optical coherence tomography study. Invest Ophthalmol Vis Sci. 2015;56(5):3218-25.

7. Mas Tur V, MacGregor C, Jayaswal R, O'Brart D, Maycock N. A review of keratoconus: Diagnosis, pathophysiology, and genetics. Surv Ophthalmol. 2017;62(6):770-83.

8. Singh T, Taneja M, Murthy S, Vaddavalli PK. Evaluation of safety and efficacy of different protocols of collagen cross linking for keratoconus. Rom J Ophthalmol. 2020;64(2):158-67.

9. Dias J, Diakonis VF, Kankariya VP, Yoo SH, Ziebarth NM. Anterior and posterior corneal stroma elasticity after corneal collagen crosslinking treatment. Exp Eye Res. 2013;116:58-62.

10. Mazzotta C, Balestrazzi A, Baiocchi S, Traversi C, Caporossi A. Stromal haze after combined riboflavin-UVA corneal collagen cross-linking in keratoconus: in vivo confocal microscopic evaluation. Clin Exp Ophthalmol. 2007;35(6):580-2.

11. Mazzotta C, Hafezi F, Kymionis G, Caragiuli S, Jacob S, Traversi C, Barabino S, Randleman JB. In Vivo Confocal Microscopy after Corneal Collagen Crosslinking. Ocul Surf. 2015;13(4):298-314.

12. Mathews PM, De Rojas JO, Rapuano PB, Zemsky CJ, Florakis GJ, Trokel SL, Suh LH. Correlation of Scheimpflug densitometry changes with clinical outcomes after corneal crosslinking. J Cataract Refract Surg. 2018;44(8):993-1002.

13. Huang J, Shen Y, Jian W, Xu H, Li M, Zhao J, Zhou X, Liao H. Two-year topographic and densitometric outcomes of accelerated (45 mW/cm(2)) transepithelial corneal cross-linking for keratoconus: a case-control study. BMC Ophthalmol. 2018;18(1):337.

14. Pircher N, Pachala M, Prager F, Pieh S, Schmidinger G. Changes in straylight and densitometry values after corneal collagen crosslinking. J Cataract Refract Surg. 2015;41(5):1038-43.

15. Bonini S, Sacchetti M, Mantelli F, Lambiase A. Clinical grading of vernal keratoconjunctivitis. Curr Opin Allergy Clin Immunol. 2007;7(5):436-41.

16. Bielory L. Allergic and immunologic disorders of the eye. Part I: immunology of the eye. J Allergy Clin Immunol. 2000;106(5):805-16.

17. Vichyanond P, Pacharn P, Pleyer U, Leonardi A. Vernal keratoconjunctivitis: a severe allergic eye disease with remodeling changes. Pediatr Allergy Immunol. 2014;25(4):314-22.

18. Bonini S, Coassin M, Aronni S, Lambiase A. Vernal keratoconjunctivitis. Eye (Lond). 2004;18(4):345-51.

19. Bonini S, Bonini S, Lambiase A, Marchi S, Pasqualetti P, Zuccaro O, Rama P, Magrini L, Juhas T, Bucci MG. Vernal keratoconjunctivitis revisited: a case series of 195 patients with long-term followup. Ophthalmology. 2000;107(6):1157-63.

20. Arif AS, Aaqil B, Siddiqui A, Nazneen Z, Farooq U. Corneal Complications And Visual Impairment In Vernal Keratoconjunctivitis Patients. J Ayub Med Coll Abbottabad. 2017;29(1):58-60.

21. Leonardi A, Bogacka E, Fauquert JL, Kowalski ML, Groblewska A, Jedrzejczak-Czechowicz M, Doan S, Marmouz F, Demoly P, Delgado L. Ocular allergy: recognizing and diagnosing hypersensitivity disorders of the ocular surface. Allergy. 2012;67(11):1327-37.

22. Le QH, Hong JX, Zhu WQ, Sun XH, Xu JJ. [Morphological characteristics of cornea in patients with vernal keratoconjunctivitis by in vivo laser scanning confocal microscopy]. Zhonghua Yan Ke Za Zhi. 2011;47(5):416-22.

23. Chan TCY, Wong ES, Chan JCK, Wang Y, Yu M, Maeda N, Jhanji V. Corneal backward scattering and higher-order aberrations in children with vernal keratoconjunctivitis and normal topography. Acta Ophthalmol. 2018;96(3):e327-e33.

24. Villani E, Dello Strologo M, Pichi F, Luccarelli SV, De Cilla S, Serafino M, Nucci P. Dry Eye in Vernal Keratoconjunctivitis: A Cross-Sectional Comparative Study. Medicine (Baltimore). 2015;94(42):e1648.

25. Micera A, Di Zazzo A, Esposito G, Sgrulletta R, Calder VL, Bonini S. Quiescent and Active Tear Protein Profiles to Predict Vernal Keratoconjunctivitis Reactivation. Biomed Res Int. 2016;2016:9672082.

26. Nebbioso M, Zicari AM, Lollobrigida V, Marenco M, Duse M. Assessment of corneal alterations by confocal microscopy in vernal keratoconjunctivitis. Semin Ophthalmol. 2015;30(1):40-3.

27. Liu M, Gao H, Wang T, Wang S, Li S, Shi W. An essential role for dendritic cells in vernal keratoconjunctivitis: analysis by laser scanning confocal microscopy. Clin Exp Allergy. 2014;44(3):362-70.

28. Leonardi A, Lazzarini D, Bortolotti M, Piliego F, Midena E, Fregona I. Corneal confocal microscopy in patients with vernal keratoconjunctivitis. Ophthalmology. 2012;119(3):509-15.

29. Modugno RL, Scalora T, Bonaldo A, Lazzarini D, Leonardi A. Corneal Microstructural Changes by Confocal Microscopy in Vernal Keratoconjunctivitis Patients Treated with Topical Cyclosporine. Ocul Immunol Inflamm. 2020:1-7.

30. Csorba A, Maneschg OA, Resch MD, Nagy ZZ. Examination of corneal microstructure in the quiescent phase of vernal keratoconjunctivitis using in vivo confocal microscopy. Eur J Ophthalmol. 2022:11206721221099778.

31. Pinxten AM, Hua MT, Simpson J, Hohenfellner K, Levtchenko E, Casteels I. Clinical Practice: A Proposed Standardized Ophthalmological Assessment for Patients with Cystinosis. Ophthalmol Ther. 2017;6(1):93-104.

32. Al-Hemidan A, Shoughy SS, Kozak I, Tabbara KF. Efficacy of topical cysteamine in nephropathic cystinosis. Br J Ophthalmol. 2017;101(9):1234-7.

33. Shams F, Livingstone I, Oladiwura D, Ramaesh K. Treatment of corneal cystine crystal accumulation in patients with cystinosis. Clin Ophthalmol. 2014;8:2077-84.

34. Biswas S, Gaviria M, Malheiro L, Marques JP, Giordano V, Liang H. Latest Clinical Approaches in the Ocular Management of Cystinosis: A Review of Current Practice and Opinion from the Ophthalmology Cystinosis Forum. Ophthalmol Ther. 2018;7(2):307-22.

35. Kocabora MS, Ozbilen KT, Altunsoy M, Ahishali B, Taskapili M. Clinicopathological features of ocular cystinosis. Clin Exp Ophthalmol. 2008;36(8):778-81.

36. Labbe A, Niaudet P, Loirat C, Charbit M, Guest G, Baudouin C. In vivo confocal microscopy and anterior segment optical coherence tomography analysis of the cornea in nephropathic cystinosis. Ophthalmology. 2009;116(5):870-6.

37. Gahl WA, Kuehl EM, Iwata F, Lindblad A, Kaiser-Kupfer MI. Corneal crystals in nephropathic cystinosis: natural history and treatment with cysteamine eyedrops. Mol Genet Metab. 2000;71(1-2):100-20.

38. Alsuhaibani AH, Khan AO, Wagoner MD. Confocal microscopy of the cornea in nephropathic cystinosis. Br J Ophthalmol. 2005;89(11):1530-1.

39. Grupcheva CN, Ormonde SE, McGhee C. In vivo confocal microscopy of the cornea in nephropathic cystinosis. Arch Ophthalmol. 2002;120(12):1742-5.

40. Richler M, Milot J, Quigley M, O'Regan S. Ocular manifestations of nephropathic cystinosis. The French-Canadian experience in a genetically homogeneous population. Arch Ophthalmol. 1991;109(3):359-62.

41. Kranitz K, Kovacs I, Mihaltz K, Sandor GL, Knorz MC, Nemeth J, Nagy ZZ. Corneal changes in progressive keratoconus after cross-linking assessed by Scheimpflug camera. J Refract Surg. 2012;28(9):645-9.

42. Naderan M, Shoar S, Kamaleddin MA, Rajabi MT, Naderan M, Khodadadi M. Keratoconus Clinical Findings According to Different Classifications. Cornea. 2015;34(9):1005-11.

43. Wollensak G, Spoerl E, Seiler T. Riboflavin/ultraviolet-a-induced collagen crosslinking for the treatment of keratoconus. Am J Ophthalmol. 2003;135(5):620-7.

44. Nemeth G, Hassan J, Modis L, Jr., Hassan Z. Long-Term Changes in Backscattered Light Measurements in Keratoconus Corneas Treated with Collagen Cross-Linking. Curr Eye Res. 2018;43(1):18-26.

45. DeLong ER, DeLong DM, Clarke-Pearson DL. Comparing the areas under two or more correlated receiver operating characteristic curves: a nonparametric approach. Biometrics. 1988;44(3):837-45.

46. Ostrovski I, Lovblom LE, Farooqi MA, Scarr D, Boulet G, Hertz P, Wu T, Halpern EM, Ngo M, Ng E, Orszag A, Bril V, Perkins BA. Reproducibility of In Vivo Corneal Confocal Microscopy Using an Automated Analysis Program for Detection of Diabetic Sensorimotor Polyneuropathy. PLoS One. 2015;10(11):e0142309.

47. Oliveira-Soto L, Efron N. Morphology of corneal nerves using confocal microscopy. Cornea. 2001;20(4):374-84.

48. Zhivov A, Stave J, Vollmar B, Guthoff R. In vivo confocal microscopic evaluation of Langerhans cell density and distribution in the normal human corneal epithelium. Graefes Arch Clin Exp Ophthalmol. 2005;243(10):1056-61.

49. Marsovszky L, Nemeth J, Resch MD, Toldi G, Legany N, Kovacs L, Balog A. Corneal Langerhans cell and dry eye examinations in ankylosing spondylitis. Innate Immun. 2014;20(5):471-7.

50. Resch MD, Marsovszky L, Nemeth J, Bocskai M, Kovacs L, Balog A. Dry eye and corneal langerhans cells in systemic lupus erythematosus. J Ophthalmol. 2015;2015:543835.

51. Marsovszky L, Resch MD, Nemeth J, Toldi G, Medgyesi E, Kovacs L, Balog A. In vivo confocal microscopic evaluation of corneal Langerhans cell density, and distribution and evaluation of dry eye in rheumatoid arthritis. Innate Immun. 2013;19(4):348-54.

52. Dehghani C, Frost S, Jayasena R, Fowler C, Masters CL, Kanagasingam Y, Jiao H, Lim JKH, Chinnery HR, Downie LE. Morphometric Changes to Corneal Dendritic Cells in Individuals With Mild Cognitive Impairment. Front Neurosci. 2020;14:556137.

53. Kheirkhah A, Rahimi Darabad R, Cruzat A, Hajrasouliha AR, Witkin D, Wong N, Dana R, Hamrah P. Corneal Epithelial Immune Dendritic Cell Alterations in Subtypes of Dry Eye Disease: A Pilot In Vivo Confocal Microscopic Study. Invest Ophthalmol Vis Sci. 2015;56(12):7179-85.

54. Resch MD, Imre L, Tapaszto B, Nemeth J. Confocal microscopic evidence of increased Langerhans cell activity after corneal metal foreign body removal. Eur J Ophthalmol. 2008;18(5):703-7.

55. Csorba A, Kránitz K, Dormán P, Popper-Sachetti A, Kiss H, Szalai I, Nagy ZZ. Factors influencing haze formation and corneal flattening, and the impact of haze on visual acuity after conventional collagen cross-linking: a 12-month retrospective study. BMC Ophthalmol. 2021;21(1):306.

56. Csorba A, Maka E, Maneschg OA, Szabó A, Szentmáry N, Csidey M, Resch M, Imre L, Knézy K, Nagy ZZ. Examination of corneal deposits in nephropathic cystinosis using in vivo confocal microscopy and anterior segment optical coherence tomography: an age-dependent cross sectional study. BMC Ophthalmol. 2020;20(1):73.

57. Yam JC, Chan CW, Cheng AC. Corneal collagen cross-linking demarcation line depth assessed by Visante OCT After CXL for keratoconus and corneal ectasia. J Refract Surg. 2012;28(7):475-81.

58. Ng AL, Chan TC, Cheng AC. Conventional versus accelerated corneal collagen cross-linking in the treatment of keratoconus. Clin Exp Ophthalmol. 2016;44(1):8-14.

59. Koller T, Mrochen M, Seiler T. Complication and failure rates after corneal crosslinking. J Cataract Refract Surg. 2009;35(8):1358-62.

60. Wittig-Silva C, Chan E, Islam FM, Wu T, Whiting M, Snibson GR. A randomized, controlled trial of corneal collagen cross-linking in progressive keratoconus: three-year results. Ophthalmology. 2014;121(4):812-21.

61. Fantes FE, Hanna KD, Waring GO, 3rd, Pouliquen Y, Thompson KP, Savoldelli M. Wound healing after excimer laser keratomileusis (photorefractive keratectomy) in monkeys. Arch Ophthalmol. 1990;108(5):665-75.

62. Takacs AI, Mihaltz K, Nagy ZZ. Corneal density with the Pentacam after photorefractive keratectomy. J Refract Surg. 2011;27(4):269-77.

63. Kim BZ, Jordan CA, McGhee CN, Patel DV. Natural history of corneal haze after corneal collagen crosslinking in keratoconus using Scheimpflug analysis. J Cataract Refract Surg. 2016;42(7):1053-9.

64. Koller T, Pajic B, Vinciguerra P, Seiler T. Flattening of the cornea after collagen crosslinking for keratoconus. J Cataract Refract Surg. 2011;37(8):1488-92.

65. Sloot F, Soeters N, van der Valk R, Tahzib NG. Effective corneal collagen crosslinking in advanced cases of progressive keratoconus. J Cataract Refract Surg. 2013;39(8):1141-5.

66. Kasai K, Kato N, Konomi K, Shinzawa M, Shimazaki J. Flattening effect of corneal cross-linking depends on the preoperative severity of keratoconus. Medicine (Baltimore). 2017;96(40):e8160.

67. Sawaguchi S, Fukuchi T, Abe H, Kaiya T, Sugar J, Yue BY. Three-dimensional scanning electron microscopic study of keratoconus corneas. Arch Ophthalmol. 1998;116(1):62-8.

68. Hayes S, Boote C, Tuft SJ, Quantock AJ, Meek KM. A study of corneal thickness, shape and collagen organisation in keratoconus using videokeratography and X-ray scattering techniques. Exp Eye Res. 2007;84(3):423-34.

69. Garzon N, Poyales F, Illarramendi I, Mendicute J, Janez O, Caro P, Lopez A, Argueso F. Corneal densitometry and its correlation with age, pachymetry, corneal curvature, and refraction. Int Ophthalmol. 2017;37(6):1263-8.

70. Lopes B, Ramos I, Ambrosio R, Jr. Corneal densitometry in keratoconus. Cornea. 2014;33(12):1282-6.

71. Baksoellah Z, Lavy I, Baydoun L, Hooijmaijers HCM, van Dijk K, Melles GRJ. Corneal Tomographic Changes After UV Cross-Linking for Corneal Ectasia (1-Year Results). Cornea. 2017;36(12):1498-502.

72. Bohm M, Shajari M, Remy M, Kohnen T. Corneal densitometry after accelerated corneal collagen cross-linking in progressive keratoconus. Int Ophthalmol. 2019;39(4):765-75.

73. Mahdavi Fard A, Daei Sorkhabi R, Khazaei M, Nader ND. The effects of collagen cross-linking on corneal density: a comparison between accelerated and conventional methods. Int Ophthalmol. 2019;39(7):1559-66.

74. Greenstein SA, Fry KL, Bhatt J, Hersh PS. Natural history of corneal haze after collagen crosslinking for keratoconus and corneal ectasia: Scheimpflug and biomicroscopic analysis. J Cataract Refract Surg. 2010;36(12):2105-14.

75. Alzahrani K, Mofty H, Lin EY, Carley F, Brahma A, Morley D, Biswas S, Hillarby MC. Corneal Imaging and Densitometry Measurements in Juvenile and Adult Keratoconus Patients to Evaluate Disease Progression and Treatment Effects After Corneal Cross-Linking. Clin Optom (Auckl). 2019;11:173-80.

76. Viswanathan D, Males J. Prospective longitudinal study of corneal collagen cross-linking in progressive keratoconus. Clin Exp Ophthalmol. 2013;41(6):531-6.

77. Toprak I, Yaylali V, Yildirim C. Factors affecting outcomes of corneal collagen crosslinking treatment. Eye (Lond). 2014;28(1):41-6.

78. Badawi AE, Abou Samra WA, El Ghafar AA. Predictive Factors of the Standard Cross-linking Outcomes in Adult Keratoconus: One-Year Follow-Up. J Ophthalmol. 2017;2017:4109208.

79. Kirgiz A, Atalay K, Cabuk KS, Kaldirim H, Taskapili M. Factors affecting visual acuity after accelerated crosslinking in patients with progressive keratoconus. Arq Bras Oftalmol. 2016;79(3):151-4.

80. Greenstein SA, Hersh PS. Characteristics influencing outcomes of corneal collagen crosslinking for keratoconus and ectasia: implications for patient selection. J Cataract Refract Surg. 2013;39(8):1133-40.

81. Gutierrez R, Lopez I, Villa-Collar C, Gonzalez-Meijome JM. Corneal transparency after cross-linking for keratoconus: 1-year follow-up. J Refract Surg. 2012;28(11):781-6.

82. Baek SH, Chang JH, Choi SY, Kim WJ, Lee JH. The effect of topical corticosteroids on refractive outcome and corneal haze after photorefractive keratectomy. J Refract Surg. 1997;13(7):644-52.

83. Vetrugno M, Maino A, Quaranta GM, Cardia L. The effect of early steroid treatment after PRK on clinical and refractive outcomes. Acta Ophthalmol Scand. 2001;79(1):23-7.

84. Kanellopoulos AJ, Cruz EM, Ang RE, Asimellis G. Higher incidence of steroid-induced ocular hypertension in keratoconus. Eye Vis (Lond). 2016;3:4.

85. Pahuja N, Shetty R, Subbiah P, Nagaraja H, Nuijts RM, Jayadev C. Corneal Densitometry: Repeatability in Eyes With Keratoconus and Postcollagen Cross-Linking. Cornea. 2016;35(6):833-7.

86. Yilmaz YC, Ipek SC, Ozer MD. Corneal and lens densitometry in patients with vernal keratoconjunctivitis. Int Ophthalmol. 2021;41(8):2667-76.

87. Smith RE, Reyes NJ, Khandelwal P, Schlereth SL, Lee HS, Masli S, Saban DR. Secondary allergic T cell responses are regulated by dendritic cell-derived thrombospondin-1 in the setting of allergic eye disease. J Leukoc Biol. 2016;100(2):371-80.

88. Manzouri B, Flynn T, Ohbayashi M, Ono SJ. The dendritic cell in allergic conjunctivitis. Ocul Surf. 2008;6(2):70-8.

89. Patel DV, Zhang J, McGhee CN. In vivo confocal microscopy of the inflamed anterior segment: A review of clinical and research applications. Clin Exp Ophthalmol. 2019;47(3):334-45.

90. Mastropasqua L, Nubile M, Lanzini M, Carpineto P, Ciancaglini M, Pannellini T, Di Nicola M, Dua HS. Epithelial dendritic cell distribution in normal and inflamed human cornea: in vivo confocal microscopy study. Am J Ophthalmol. 2006;142(5):736-44.

91. Hamrah P, Huq SO, Liu Y, Zhang Q, Dana MR. Corneal immunity is mediated by heterogeneous population of antigen-presenting cells. J Leukoc Biol. 2003;74(2):172-8.

92. Zhivov A, Stave J, Vollmar B, Guthoff R. In vivo confocal microscopic evaluation of langerhans cell density and distribution in the corneal epithelium of healthy volunteers and contact lens wearers. Cornea. 2007;26(1):47-54.

93. Massingale ML, Li X, Vallabhajosyula M, Chen D, Wei Y, Asbell PA. Analysis of inflammatory cytokines in the tears of dry eye patients. Cornea. 2009;28(9):1023-7.

94. Dana R. Comparison of topical interleukin-1 vs tumor necrosis factor-alpha blockade with corticosteroid therapy on murine corneal inflammation, neovascularization, and transplant survival (an American Ophthalmological Society thesis). Trans Am Ophthalmol Soc. 2007;105:330-43.

95. Chigbu DI, Labib BA. Immunopharmacology in Vernal Keratoconjunctivitis: Current and Future Perspectives. Pharmaceuticals (Basel). 2021;14(7).

96. Dufier JL, Dhermy P, Gubler MC, Gagnadoux MF, Broyer M. Ocular changes in long-term evolution of infantile cystinosis. Ophthalmic Paediatr Genet. 1987;8(2):131-7.

97. Melles RBS, J.A.; Rao N.A.; Katz, B. Spatial and temporal sequence of corneal crystal deposition in nephropathic cystinosis. Am J Ophthalmol. 1987;104(6):598-604.

98. Sanderson PO, Kuwabara, T., Stark, W.J., Wong, V.G., Collins, E.M. Cystinosis. A clinical, histopathologic, and ultrastructural study. Arch Ophthalmol. 1974 91(4):270-4.

99. Simpson J, Nien CJ, Flynn K, Jester B, Cherqui S, Jester J. Quantitative in vivo and ex vivo confocal microscopy analysis of corneal cystine crystals in the Ctns knockout mouse. Mol Vis. 2011;17:2212-20.

100. Park M, Helip-Wooley A, Thoene J. Lysosomal cystine storage augments apoptosis in cultured human fibroblasts and renal tubular epithelial cells. J Am Soc Nephrol. 2002;13(12):2878-87.

101. Emma F, Nesterova G, Langman C, Labbe A, Cherqui S, Goodyer P, Janssen MC, Greco M, Topaloglu R, Elenberg E, Dohil R, Trauner D, Antignac C, Cochat P, Kaskel F, Servais A, Wuhl E, Niaudet P, Van't Hoff W, Gahl W, Levtchenko E. Nephropathic cystinosis: an international consensus document. Nephrol Dial Transplant. 2014;29(Suppl 4):87-94.

102. Kenyon KR, Sensenbrenner JA. Electron microscopy of cornea and conjunctiva in childhood cystinosis. Am J Ophthalmol. 1974;78(1):68-76.

103. Gahl WA, Thoene JG, Schneider JA. Cystinosis. N Engl J Med. 2002;347(2):111-21.

104. Dixon P, Christopher K, Chauhan A. Potential role of stromal collagen in cystine crystallization in cystinosis patients. Int J Pharm. 2018;551(1-2):232-40.

105. Kaiser-Kupfer MI, Caruso RC, Minkler DS, Gahl WA. Long-term ocular manifestations in nephropathic cystinosis. Arch Ophthalmol. 1986;104(5):706-11.

106. Tsilou ET, Rubin BI, Reed GF, Iwata F, Gahl W, Kaiser-Kupfer MI. Age-related prevalence of anterior segment complications in patients with infantile nephropathic cystinosis. Cornea. 2002;21(2):173-6.

107. Pescina S, Carra F, Padula C, Santi P, Nicoli S. Effect of pH and penetration enhancers on cysteamine stability and trans-corneal transport. Eur J Pharm Biopharm. 2016;107:171-9.

108. Makuloluwa AK, Shams F. Cysteamine hydrochloride eye drop solution for the treatment of corneal cystine crystal deposits in patients with cystinosis: an evidence-based review. Clin Ophthalmol. 2018;12:227-36.

109. Liang H, Labbe A, Le Mouhaer J, Plisson C, Baudouin C. A New Viscous Cysteamine Eye Drops Treatment for Ophthalmic Cystinosis: An Open-Label Randomized Comparative Phase III Pivotal Study. Invest Ophthalmol Vis Sci. 2017;58(4):2275-83.

9. Bibliography of the candidate's publications

9.1. Publications related to the PhD thesis

1. **Csorba A**, Kranitz K, Dorman P, Popper-Sachetti A, Kiss HJ, Szalai I, Nagy ZZ. Factors influencing haze formation and corneal flattening, and the impact of haze on visual acuity after conventional collagen cross-linking: a 12-month retrospective study. BMC Ophthalmol. 2021;21(1):306. **IF: 2.086**
2. **Csorba A**, Maneschg OA, Resch MD, Nagy ZZ. Examination of corneal microstructure in the quiescent phase of vernal keratoconjunctivitis using in vivo confocal microscopy. Eur J Ophthalmol. 2023;33(1):196-202. **IF: 1.922**
3. **Csorba A**, Maka E, Maneschg OA, Szabo A, Szentmary N, Csidey M, Resch MD, Imre L, Knezy K, Nagy ZZ. Examination of corneal deposits in nephropathic cystinosis using in vivo confocal microscopy and anterior segment optical coherence tomography: an age-dependent cross sectional study. BMC Ophthalmol. 2020;20(1):73. **IF: 2.209**

Σ Impact factor: 6.217

9.2. Publications not related to the PhD thesis

1. Nagy ZZ, **Csorba A**, Dorman P, Kiss HJ. A szürkehályog-sebészet helyzete Magyarországon 2018-ban. A „Katarakta regiszter" eredményeinek összegzése. Szemészet. 2018;156 (4):228-34.
2. **Csorba A**, Kiss H, Nagy ZZ. Extrakapszuláris lencse extrakció szövődményeként kialakult cisztikus filtrációs párna. Szemészet. 2018;155:205-7.
3. **Csorba A**, Soproni A, Maneschg O, Nagy ZZ, Szamosi A. A kortikoszteroidtartalmú szemcseppek alkalmazása gyermekkori allergiás szembetegségek kezelésében [Application of corticosteroid eye drops for allergic eye disease in children]. Orv Hetil. 2019;160(9):329-37. **IF: 0.497**
4. Maneschg O, Knezy K, Maka E, **Csorba A**, Szabo V, Nagy ZZ. Külső szemizmok ínhosszabbítása szarvasmarha-pericardium grafttal [Tutopatch®] nagyfokú konszekutív horizontális kancsalság esetén: Esetismertetések. Szemészet. 2019;156(3):185-190

5. Hollo CT, Mihaltz K, Kurucz M, **Csorba A**, Kranitz K, Kovacs I, Nagy ZZ, Erdei G. Objective quantification and spatial mapping of cataract with a Shack-Hartmann wavefront sensor. Sci Rep. 2020;10(1):12585. **IF: 4.380**
6. Szalai I, Palya F, **Csorba A**, Toth M, Somfai GM. The Effect of Physical Exercise on the Retina and Choroid. Klin Monbl Augenheilkd. 2020;237(4):446-9. **IF: 0.700**
7. Nagy ZZ, Dorman P, **Csorba A**, Kovacs K, Benyo F, Istvan L, Kiss HJ. A hályogsebészet helyzete Magyarországon 2020-ban a "Katarakta regiszter" eredményeinek összegzése. Szemészet. 2021;158(3):138-43.
8. Kormanyos K, Kovacs K, Nemeth O, Toth G, Sandor GL, **Csorba A**, Czako CN, Langenbucher A, Nagy ZZ, Varga G, Gopcsa L, Mikala G, Szentmary N. A monoklonális gammopathia szemészeti jelei és szövődményei. 42 beteg 84 szemének vizsgálata [Ocular signs and comorbidities in monoclonal gammopathy Analysis of 84 eyes of 42 subjects]. Orv Hetil. 2021;162(38):1533-40. **IF: 0.707**
9. Vegh A, Magda DP, Kilin F, **Csorba A**, Resch M, Nagy ZZ, Szabo A. Sejtszintű képalkotás a retina in vivo vizsgálatában: jelen és jövő [In vivo cellular imaging of the retina: present and future]. Orv Hetil. 2021;162(22):851-60. **IF: 0.707**
10. Szentmary N, Kormányos K, Toth G, Sandor G, Nemeth O, **Csorba A**, Czako CN, Kovacs K, Nagy ZZ, Varga G, Gopcsa L, Mikala G. Szemészeti tünetek és szemészeti társbetegségek monoklonális gammopathiával járó kórképekben. Hematológia-Transzfuziológia 2021;54 (2):82-8.
11. Kormanyos K, Kovacs K, Nemeth O, Toth G, Sandor GL, **Csorba A**, Czako CN, Langenbucher A, Nagy ZZ, Varga G, Gopcsa L, Mikala G, Szentmary N. Ocular Signs and Ocular Comorbidities in Monoclonal Gammopathy: Analysis of 80 Subjects. J Ophthalmol. 2021;2021:9982875. **IF: 1.974**
12. Kovacs B, Lang B, Takacsi-Nagy A, Horvath G, Czako CN, **Csorba A**, Kiss HJ, Szalai I, Nagy ZZ, Kovacs I. Meibom-mirigy-diszfunkció és a száraz szem: Diagnosztikai és kezelési lehetőségek [Meibomian gland dysfunction and dry eye: Diagnosis and treatment]. Orv Hetil. 2021;162(2):43-51. **IF: 0.707**
13. Kormanyos K, Kovács K, Nemeth O, Toth G, Sandor GL, **Csorba A**, Czako CN, Modis L Jr, Langenbucher A, Nagy ZZ, Varga G, Gopcsa L, Mikala G, Szentmary N. Corneal Densitometry and In Vivo Confocal Microscopy in Patients with

Monoclonal Gammopathy-Analysis of 130 Eyes of 65 Subjects. J Clin Med. 2022;11(7). **IF: 4.964**

14. Szalai I, **Csorba A**, Palya F, Jing T, Horvath E, Bosnyak E, Gyore I, Nagy ZZ, DeBuc DC, Toth M, Somfai GM, Grzybowski A. The assessment of acute chorioretinal changes due to intensive physical exercise in young adults. PLoS One. 2022;17(5):e0268770. **IF: 3.752**
15. Szalai I, **Csorba A**, Jing T, Horvath E, Bosnyak E, Gyore I, Nagy ZZ, DeBuc DC, Toth M, Somfai GM. The Assessment of Acute Chorioretinal Changes Due to Intensive Physical Exercise in Senior Elite Athletes. J Aging Phys Act. 2022:1-9. **IF: 2.109**
16. **Csorba A**, Nagy ZZ, Maneschg O. Szezonális allergiás szemészeti betegségek és kezelésük gyermekeknél. Gyermekgyógyászati Továbbképző Szemle. 2022; 1585-4396:27 (4):107-10.
17. Istvan L, Benyo F, **Csorba A**, Jimoh IJ, Gal A, Molnar M, Nagy ZZ, Szabo V. Cornealis polymegathismus és retinalis pigmenthám-eltérések MELAS-szindrómában. Szemészet. 2022;0039-8101: 159 (2):69-75.
18. Vegh A, **Csorba A**, Koller A, Mohammadpour B, Killik P, Istvan L, Magyar M, Fenesi T, Nagy ZZ. Presence of SARS-CoV-2 on the conjunctival mucosa in patients hospitalized due to COVID-19: Pathophysiological considerations and therapeutic implications. Physiol Int. 2022;109(4):475-85. **IF: 1.697**
19. Sipos B, Budai-Szucs M, Kokai D, Orosz L, Burian K, **Csorba A**, Nagy ZZ, Balogh GT, Csoka I, Katona G. Erythromycin-loaded polymeric micelles: In situ gel development, in vitro and ex vivo ocular investigations. Eur J Pharm Biopharm. 2022;180:81-90. **IF: 5.589**
20. **Csorba A**, Kranitz K, Dorman P, Kiss HJ, Nagy ZZ. Cross-linking kezelést követő cornealis denzitometria keratoconusos betegekben. Szemészet. 2022;159(4):163-7.
21. **Csorba A**, Maka E, Szabo A, Kelen K, Reusz G, Nagy ZZ. Ciszteamintartalmú szemcsepp alkalmazása cystinosisban [Ocular treatment of cystinosis with eye drop containing cysteamine]. Orv Hetil. 2022;163(21):846-52. **IF: 0.707**

22. **Csorba A**, Katona G, Budai-Szucs M, Balogh-Weiser D, Fadda AM, Caddeo C, Takacs AI, Matyus P, Balogh GT, Nagy ZZ. Effect of liposomal formulation of ascorbic acid on corneal permeability. Sci Rep. 2023;13(1):3448. **IF: 4.997**
23. Vincze A, Facsko R, Budai-Szucs M, Katona G, Gyarmati B, **Csorba A**, Zelko R, Nagy ZZ, Szente L, Balogh GT. Cyclodextrin-enabled nepafenac eye drops with improved absorption open a new therapeutic window. Carbohydr. Polym. 2023; 310: 120717. **IF: 10.723**
24. Naray A, Csidey M, Keki-Kovacs K, Nemeth O, Knezy K, Bausz M, Szigeti A, **Csorba A**, Kormanyos K, Szabo D, Stachon T, Corton M, Tory K, Nagy ZZ, Maka E, Szentmary N. Congenitalis aniridia – egy spektrumbetegség magyarországi adatai [Congenital aniridia - Hungarian data of a spectrum disease]. Orv Hetil. 2023;164(4):148-55. **IF: 0.707**
25. Sonkodi B, **Csorba A**, Marsovszky L, Balog A, Kopper B, Nagy ZZ, Resch MD. Evidence of Disruption in Neural Regeneration in Dry Eye Secondary to Rheumatoid Arthritis. Int J Mol Sci. 2023;24(8). **IF: 6.208**

DOI:10.14753/SE.2024.2880

10. Acknowledgements

First and foremost, I owe a debt of gratitude to my supervisor, **Zoltán Zsolt Nagy**, who has been supporting my research for years, allowed me to acquire professional knowledge in ophthalmology, and sparked my interest in corneal diseases.

I truly appreciate the unwavering support, advice, and selflessness of **Otto Alexander Maneschg**. His constant positive attitude helped me through the most difficult periods.

I express my gratitude to **Erika Maka**, and I would like to thank her for trusting in my work from the outset and allowing me to collaborate with her on one of the most interesting topics.

Many thanks to **László Imre**, who was my mentor in the interpretation of confocal images. Thanks for his unique ideas, clear explanations, and the time to think together.

I am grateful to **Kinga Kránitz**, who generously sacrificed her own free time to familiarize me with statistical analyses and provided invaluable guidance and ideas.

I would also like to thank to **Miklós Dénes Resch** for his valuable suggestions.

Additionally, I extend a special thank you to all of my colleagues at the Department of Ophthalmology of Semmelweis University for their unwavering assistance and support.

Last, but not least, I would like to express my heartfelt gratitude for the unwavering support of my family, especially my beloved husband, who provides a constant foundation of support and balance in my life. His patience, encouragement, and belief in my success kept me inspired during this challenging journey.